Previously, we reported that the single amino acid of Leu868 is responsible for base selection and translesion of DNA synthesis in *Saccharomyces cerevisiae* pol α [7]. In that study, L868F pol α showed a DNA replication fidelity 570-fold lower than that of the wild-type and catalyzed efficient bypass of DNA lesions more efficiently than the wild-type. In yeast cells, *pol1L868F* conferred a mutator phenotype, and DNA pol α-dependent replication errors were recognized and repaired by mismatch repair. Because the human pol α mutant also showed low fidelity *in vitro*, this mutant pol may provide a means to study the role of error prevention steps for pol α in human cells.

In the present study, we investigated the biochemical properties of the human counterpart of L864F pol α. We expressed mutant pol α in the human cell line HCT116 and examined whether L864F pol α causes a mutator phenotype.

2. Methods

2.1. Enzyme overexpression and purification

Human *POLA1* was PCR-amplified from a cDNA clone, which was originally provided by Dr. Heinz-Peter Nasheuer (Natl. Univ., Ireland), and cloned into pcDNA3.1 (Invitrogen, Carlsbad, CA) at the *Eco*RI and *Xba*I sites [17]. The CTA → TTC mutation was introduced to construct *pola1L864F* [7]. His_6-tagged wild-type and L864F pol α were expressed in insect cells, then purified using a BAC-TO-BAC HT Baculovirus Expression System (Invitrogen), as previously described [7,18,19]. *Escherichia coli* DH10bac (Invitrogen) was transformed with pFastBac HTb vectors carrying either wild-type or *pola1L864F* ORF. A single colony containing the recombinant bacmid was picked, inoculated into 2 mL of 2 × YT, and cultured at 37 °C overnight. The bacmid DNA was then purified and transfected into Sf9 cells according to the supplier's instructions (Invitrogen).

At 72 h postinfection, cells (2.5×10^7) were harvested by centrifugation at 500 × *g*, then lysed and homogenized in lysis buffer [50 mM Tris–HCl (pH 8.0), 100 mM KCl, 20 mM imidazole, 5 mM 2-mercaptoethanol, 1 mM PMSF, and 1% Nonidet P-40] at 4 °C. The lysate was incubated on ice for 1 h and centrifuged at 25,000 × *g* for 10 min. The supernatant was loaded onto a Ni-resin column (Novagen/Merck, His-Bind Resin, Darmstadt, Germany) equilibrated with buffer A [20 mM Tris–HCl (pH 8.0), 500 mM KCl, 20 mM imidazole, 5 mM 2-mercaptoethanol, 10% glycerol]. The column was washed sequentially with 10 ml of buffer A, 2 ml of buffer B [20 mM Tris–HCl (pH 8.0), 1 M KCl, 5 mM 2-mercaptoethanol, 10% glycerol], and 2 ml of buffer A. The enzyme was eluted with 5 ml of elution buffer [20 mM Tris–HCl (pH 8.0), 100 mM KCl, 100 mM imidazole, 5 mM 2-mercaptoethanol, 10% glycerol] and 0.5-ml fractions were collected. Peak fractions were dialyzed against 500 ml of dialysis buffer I [30% glycerol, 50 mM Tris–HCl (pH 8.0), 2 mM 2-mercaptoethanol] for 4 h, followed by dialysis buffer II [50% glycerol, 50 mM Tris–HCl (pH 8.0), 2 mM 2-mercaptoethanol] for 4 h. The purity of the proteins was then analyzed using SDS-PAGE (Fig. 1). Protein concentrations were determined using the Bradford dye-binding method (BioRad, Hercules, CA).

2.2. M13mp2 gap filling assay

Replication errors were quantified using an M13mp2 forward mutation assay as described previously [4,5,7,19]. A gapped M13mp2 substrate was constructed with a single-strand gap in the *lacZα* complementary region. The reaction mixture contained 5 U of WT or L864F pol α, 400 ng gapped M13mp2, 20 mM Tris–HCl (pH 8.0), 2 mM dithiothreitol, 10 mM $MgCl_2$, 50 mM KCl, and 0.2 mM dNTPs. Reactions were conducted at 37 °C for 10 min and each reaction product was transfected into *E. coli*. Mutant plaques were identified by color. The background mutation rate was subtracted prior to calculating the error frequencies. The nucleotide sequences of the mutants were determined using an oligonucleotide primer, 5′-CAGCCAGCTTTCCGGCA-3′.

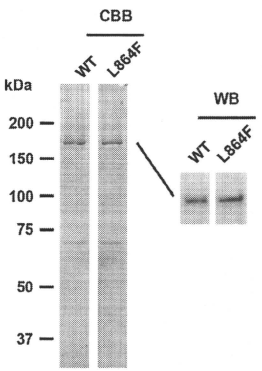

Fig. 1. Purity of wild-type and L864F pol α. Pol α was expressed and purified as described in Section 2. Wild-type (WT) and L864F (LF) pol α preparations were analyzed by 10% polyacrylamide gel electrophoresis, followed by Coomassie brilliant blue staining (CBB) or Western blotting (WB) analysis. The positions of the size markers are also shown.

2.3. Primer extension assay

A 16-mer DNA primer (5′-CACTGACTGTATGATG) was ^{32}P-labeled at the 5′ terminus using T4 polynucleotide kinase and [γ-^{32}P]ATP, then annealed with a 1.2-fold molar excess of complementary 30-mer with or without the DNA lesion (Etheno-A, O^6-methyl-G, O^4-methyl-T, or 8-oxo-G). The 30-mer nucleotide sequence was 5′-CTCGTCAGCATCXCATCATACAGTCAGTG-3′, where X represents the damaged nucleotide. For an abasic template, the underlined X was replaced with the abasic analog. Next, 10 μl of reaction mixture containing either 72 ng of WT or 26 ng of L864F pol α, along with 40 nM of primer/template, 50 mM potassium-phosphate buffer (pH 7.2), 2 mM β-mercaptoethanol, 5 mM $MgCl_2$, 0.1 mg/ml of bovine serum albumin (BSA), and 20 μM of either one or all four dNTPs. The reactions were conducted at 37 °C for 5 min and each reaction product was analyzed on a 14% polyacrylamide gel containing 8 M urea, and visualized by X-ray film exposure [7,18,19].

2.4. Steady state kinetics

The incorporation efficiencies for correct and incorrect nucleotides, and extension efficiencies for matched and mismatched primer termini were determined as described previously, with some modifications [7,18]. A ^{32}P-labeled 14 mer (5′-GCTCACAATTCCAC) or 15 mer (5′-GCTCACAATTCCACA or 5′-GCTCACAATTCCACG) primer was annealed to each 20-mer template (5′-TGTTGTGTGGAATTGTGAGC) that corresponded to the −10 to +10 area of the *LacZα* complementation gene. For translesion kinetics, a ^{32}P-labeled 16 mer (5′-CACTGACTGTATGATG) or 17 mer (5′-CACTGACTGTATGATGC or 5′-CACTGACTGTATGATGT) was annealed with either a non-damaged or O^6-methyl-G template. The ^{32}P-labeled template-primer (40 nM) was incubated for 5–30 min at 37 °C in a reaction mixture (10 μl) containing 50 mM potassium-

phosphate buffer (pH 7.2), 2 mM β-mercaptoethanol, 5 mM $MgCl_2$, 0.1 mg/ml of BSA, and various concentrations of dNTP, along with an amount of enzyme that provided less than 20% template-primer utilization. To obtain that result, the enzyme amounts were varied and monitored for the optimum concentration according to the primer-template and substrate combinations, i.e., 18–180 ng and 6.6–52 ng of WT and L864F pol α, respectively. The reaction products were separated on a 14% polyacrylamide gel containing 8 M urea and analyzed using a Fuji Image Analyzer (Fuji Film, Tokyo, Japan). Data were analyzed on Hanes–Woolf plots, and apparent K_m and k_{cat} (average of 3 measurements) were calculated from the graphs.

2.5. Pol α overexpression

A 1.2-μg amount of pcDNA3.1 carrying human *POLA1* or *pola1L864F* was transfected into 4×10^5 HCT116 or T98G cells, and cultured with 1 mg/ml of G418 (Invitrogen-Life Technologies, Grand Island, NY) in 10% fetal bovine serum-supplemented DMEM medium. G418 resistant clones were monitored for the expression of pol α and used for HPRT mutation assays. In some assays, pol α was transiently expressed in HCT116 cells. Prior to the experiments, cells were cultured in HAT (hypoxanthine, aminopterin, and thymidine; Sigma–Aldrich, St. Louis, MO) and 10% fetal bovine serum-supplemented DMEM medium for 1 week at 37 °C in a 5% CO_2 incubator, followed by a 3-week culture in HT (hypoxanthine and thymidine; Sigma–Aldrich) and 10% fetal bovine serum-supplemented DMEM medium. A 4.8-μg amount of pcDNA3.1 carrying human *POLA1* or *pola1L864F*, and 1.2 μg of puromycin-resistant plasmid were transfected into HCT116 cells (2×10^6) using 18 μl of FuGENE and 600 μl of Opti-MEM (Roche, Basel, Switzerland), and incubated for 48 h with 10% fetal bovine serum-supplemented DMEM medium. The transfected cells were cultured for 3 days with 10% fetal bovine serum-supplemented DMEM medium containing 1.5 μg/ml puromycin and puromycin-resistant cells were used for the *HPRT* mutation assays.

2.6. PCR detection of integrated DNA and POLA1/pola1L864F mRNA

The primer sequences used for the detection of plasmid-borne *POLA1*/*pola1L864F* were HaTF15 (5′-CACTCTGGCCCTAAATGCTC) and pcDNAR1 (5′-CTAGAAGGCACAGTCGAGGC), which anneal with the 3′ terminus region of human *POLA1*/*pola1L864F* cDNA and downstream of the multi-cloning site of pcDNA3.1. Thirty cycles of PCR were carried out as follows: 95 °C for 30 s, 50 °C for 30 s, and 72 °C for 2 min. Either genomic DNA or cDNA was used for the template. Reaction products were analyzed using 2% agarose gel electrophoresis. In some experiments, PCR products were digested by *Xba* I prior to electrophoresis.

2.7. Measurement of cell growth

Cell growth was measured by plating cells at a density of 1×10^5 cells in 3.5-cm dishes on day 0 and then performing MTT assays for up to 6 days [20].

2.8. HPRT mutation assays

Establishment of HCT116 cells stably transfected with *POLA1* or *pola1L864F* was performed as described above. Prior to the experiments, cells were cultured in HAT and 10% fetal bovine serum supplemented with DMEM, as described above. Each stable clone was seeded into 15 wells of three 6-well plates (100 cells/well) and incubated until an adequate cell number was obtained. Next, 5×10^5 cells were plated and incubated in 10-cm plates containing 5 μg/ml of 6-thioguanine (6-TG; Sigma–Aldrich) for 10–12 days. To determine plating efficiency, 1×10^3 cells from each clone were also seeded in 10-cm plates. The method used for calculation of the mutation rate has been described [21].

To determine mutant frequency, HCT116 cells were transiently transfected with *POLA1*/*pola1L864F* and prepared as described above. Next, 5×10^5 cells were plated and incubated in 10-cm plates with 10% fetal bovine serum-supplemented DMEM medium containing 5 μg/ml of 6-TG for 10 days. In a parallel experiment, 1×10^3 cells were also plated in 10-cm plates and incubated in 6-TG free medium for 10 days to determine plating efficiency. To determine mutant frequency, the number of 6-TG-resistant colonies was divided by 5×10^5, followed by correction for plating efficiency. Values are presented with SD and show the average of five independent results.

To determine methyl methanesulfonate (MMS; Sigma–Aldrich) sensitivity, HCT116 cells were treated with various concentrations of MMS and cultured for 10 days. In the next experiment, 5×10^5 cells with a transient expression of pol α were plated in 10-cm plates, incubated for 24 h, and treated with 100 μg/ml of MMS for 1 h to measure the mutant frequency. Under these conditions, 80% of the cells were expected to survive and form colonies. The cells were washed twice with PBS and incubated in 10-cm plates containing 5 μg/ml of 6-TG for 10 days. For determination of plating efficiency, 1×10^3 cells were incubated in 6-TG free medium for 10 days. Mutant frequency was calculated as described above.

2.9. Western blotting analysis

An 80-μg amount of total cell extract was separated on a 7.5% SDS-polyacrylamide gel and transferred to Immobilion-P filters (Millipore Corp., Bedford, MA). The expressions of pol α (catalytic subunit) and Lamin B were detected using the polyclonal goat antibodies anti-DNA pol α (G-16) and anti-Lamin B (C-20) (Santa Cruz Biotechnology, Santa Cruz, CA), respectively, while that of α-tubulin was detected using the monoclonal mouse antibody anti-α-tubulin (sc-5286) (Santa Cruz Biotechnology, Santa Cruz, CA). Secondary antibodies utilized were anti-goat IgG-HRP (sc-2020) (Santa Cruz Biotechnology, Santa Cruz, CA) and anti-mouse IgG-HRP (Cell Signaling Technology, Beverly, MA). In some experiments, an Enhanced Chemiluminescence System (Amersham, Buckinghamshire, UK) was employed.

3. Results

3.1. Fidelity of human L864F pol α

A human pol α mutant carrying the L864F substitution was reported to have reduced base selection ability while DNA polymerase activity was maintained [7]. Using this mutant, we investigated whether the base selection step plays a role in human cells. In order to understand the mutagenic character of L864F pol α *in vitro*, we performed an *in vitro LacZα* forward mutation assay. In that analysis, L864F pol α showed a mutation rate 180-fold greater than that of the wild-type (Table 1; 6.6×10^{-5} vs. 1.2×10^{-2}). As with its *S. cerevisiae* counterpart [7], our mutant generated base substitution errors throughout the target DNA sequence (Table 1 and Fig. 2) and showed relatively high transversions, 53% transversions and 34% transitions, whereas wild-type pol α generated those at rates of 27% and 48%, respectively (Table 1). L864F pol α also generated frameshift errors, with a 330-fold higher rate of +1 insertions and a 100-fold higher rate of −1 deletions than wild-type pol α (Table 1). We also found that both *S. cerevisiae* and human pol α mutants often generated single-base deletions in non-run sequences, i.e., 36/64 [7] and 19/49 (Fig. 2), respectively. On the

Table 1
Types of errors by human wild-type and L864Fpol α in *lacZα* forward mutation assays.

Error type	Wild-type pol α			L864F pol α			Fold increase (L864F/WT)
	N	%	Error rate ($\times 10^{-5}$)	*N*	%	Error rate ($\times 10^{-5}$)	
All errors	107	100	6.6	618	100	1200	180
Base substitutions	81	76	5.4	537	87	1100	200
Transitions	52	49	3.5	210	34	420	120
T→C	22	21	1.5	65	11	130	88
C→T	17	16	1.1	50	8	99	87
A→G	0	0	0	12	2	24	>360
G→A	13	12	0.87	83	13	160	190
Transversions	29	27	1.9	327	53	650	330
T→A	1	1	0.067	52	8	100	1500
T→G	7	7	0.47	47	8	93	200
A→T	10	9	0.67	111	18	220	330
A→C	0	0	0	7	1	14	>210
G→T	4	4	0.27	20	3	40	150
G→C	1	1	0.067	13	2	26	390
C→A	6	6	0.4	74	12	150	370
C→G	0	0	0	3	0	5.9	>88
Frameshifts	26	24	1.2	81	13	160	130
1-Base deletions	21	20	0.98	49	8	97	100
2-Base deletions	1	1	0.048	0	0	0	0
1-Base insertions	4	4	0.19	31	5	61	330
2-Base insertions	0	0	0	1	0	2.0	>30

other hand, N→T base substitutions, the most frequently observed base substitutions in *S. cerevisiae*, were not dominantly seen in human L864F pol α (Table 1). Unlike its *S. cerevisiae* counterpart, no single tandem base deletion or large deletion was generated by human L864F pol α (Table 1).

We also compared the base substitution properties between wild-type and L864F pol α by determining single nucleotide incorporation and extension kinetic values at one of the mutation hot spots in the M13mp2 sequence. At the nucleotide incorporation step, L864F pol α showed a misincorporation efficiency of incorrect

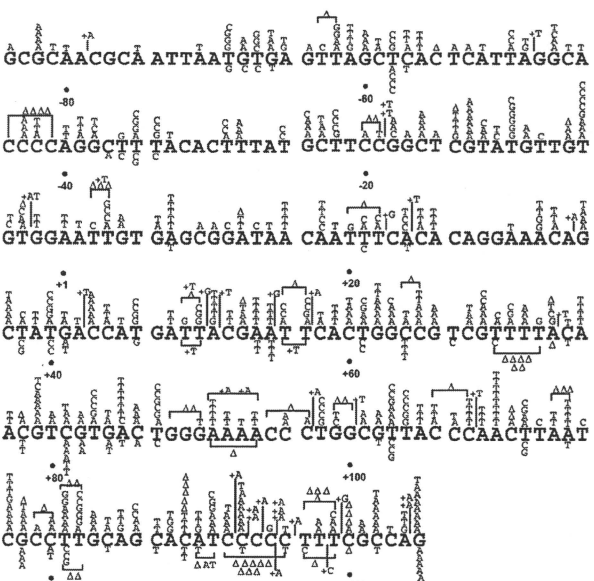

Fig. 2. Wild-type and L864F pol α mutation spectra in M13mp2 *lacZα*. The M13mp2 DNA sequence is shown. Base substitutions and frameshifts produced by L864F pol α are indicated above the M13mp2 sequence, and those produced by wild-type pol α are indicated below the sequence. The −1 and +1 frameshift mutations are indicated by Δ (deletion) and +N (insertion), respectively. For a frameshift in a run sequence, the symbol is centered in the run.

Table 2
Incorporation kinetics of WT and L864F pol α.

Enzyme	Template: dNTP	K_m (μM)	k_{cat} (min^{-1})	k_{cat}/K_m ($\mu M^{-1}\ min^{-1}$)	$f_{inc\text{-}1}$ [a]	$f_{inc\text{-}2}$ [b]
WT pol α	T:dATP	1.8 ± 0.08	033 ± 0.01	0.18 ± 0.01	1	
	T:dGTP	1.200 ± 275	(3.9 ± 0.94) × 10^{-3}	(32 ± 0.86) × 10^{-6}	1.8 × 10^{-5}	1
L864F pol α	T:dATP	0.31 ± 0.01	0.39 ± 0.03	1.3 ± 0.12	1	
	T:dGTP	170 ± 33	0.69 ± 0.21	(4.1 ± 1.1) × 10^{-3}	3.3 × 10^{-3}	180

[a] Relative incorporation efficiency to $k_{cat}/K_{m(T:dATP)}$.
[b] Relative incorporation efficiency to $f_{inc\text{-}1(T:dGTP,\ WT)}$.

Table 3
Extension kinetics of WT and L864F pol α.

Enzyme	Template: primer terminus	K_m (μM)	k_{cat} (min^{-1})	k_{cat}/K_m ($\mu M^{-1}\ min^{-1}$)	$f_{inc\text{-}1}$ [a]	$f_{inc\text{-}2}$ [b]
WT pol α	T:dA	5.4 ± 0.32	0.077 ± 0.029	0.014 ± 0.005	1	
	T:dG	940 ± 160	(8.4 ± 2.1) × 10^{-3}	(9.2 ± 2.9) × 10^{-6}	6.6 × 10^{-4}	1
L864F pol α	T:dA	2.8 ± 0.23	0.49 ± 0.16	0.17 ± 0.05	1	
	T:dG	17 ± 5.4	0.38 ± 0.05	0.024 ± 0.008	0.14	210

[a] Relative extension efficiency to $k_{cat}/K_{m(T:dA)}$.
[b] Relative extension efficiency to $f_{ext\text{-}1(T:dG,\ WT)}$.

dGMP at a rate 180-fold higher than the wild-type (Table 2). L864F pol α also showed an ability to extend the mismatched primer by 210-fold more than the wild-type (Table 3).

3.2. Translesion DNA synthesis activity

Amino acids located at corresponding positions regulate DNA replication fidelity as well as translesion activity in both replicative and translesion pols [7,22]. In accord with previous results [7], the present human L864F pol α showed efficient DNA synthesis over the abasic site (Fig. 3). Furthermore, L864F pol α elongated DNA over the alkylated damages of etheno-A, O^4-methyl-T, and O^6-methyl-G more efficiently than the wild-type (Fig. 3).

In addition, we quantitated the translesion activities of wild-type and L864F pol α at the O^6-methyl-G site. Since both wild-type and L864F pol α preferred dCMP or dTMP incorporation at this lesion (Fig. 3B), these two nucleotides were chosen for kinetic evaluation. In accord with the results of other B-family DNA polymerases [23,24], each enzyme showed similar dCMP and dTMP incorporation efficiencies; 0.034 and 0.025, respectively, for wild-type vs. 0.25 and 0.30, respectively, for L864F pol α (Table 4, $f_{inc\text{-}1}$). Each enzyme also extended O^6-methyl-G:dC and O^6-methyl-G:dT with similar efficiencies, 0.018 and 0.038, respectively, for wild-type vs. 0.47 and 0.50, respectively, for L864F pol α (Table 5, $f_{ext\text{-}1}$). However, we also found that L864F pol α incorporated dCMP or dTMP (Table 4, $f_{inc\text{-}2}$), and extended the resultant primer termini (Table 5, $f_{ext\text{-}2}$) 7.4–26-fold more efficiently than the wild-type. These data indicate that L864F pol α performed translesion DNA synthesis with relatively ease over the O^6-methyl-G site.

3.3. HPRT mutation assay using stable clones

We studied mutant frequencies using cells with wild-type or *pola1L864F* transfection. Initially, we prepared stable clones using a mismatch repair-proficient cell line of T98G. However, with *pola1L864F* transfection we observed only a single 6-TG-resistant colony in a survey of 72 plates (3.6 × 10^7 cells) and no colony with the wild-type. Since the *HPRT* mutation rates were low, we did not perform any further experiment using these clones.

Yeast pol α errors are corrected by mismatch repair [7,25], thus we established clones using the mismatch repair-deficient cell line HCT116. Integration of the pol α genes was confirmed by PCR,

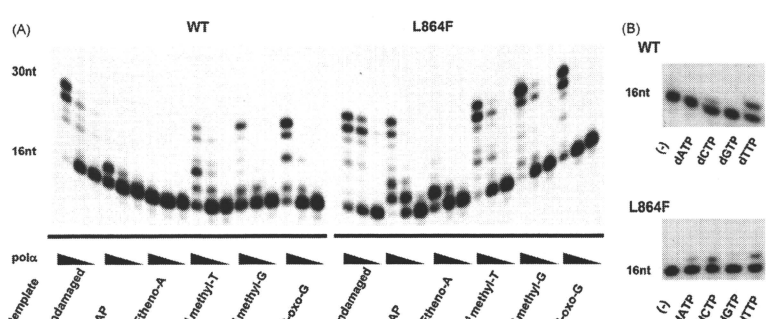

Fig. 3. Translesion synthesis by wild-type (WT) and L864F pol α. (A) For translesion DNA synthesis, enzymes were incubated with an undamaged or damaged template, as indicated. The primer terminus was properly base-paired to the nucleotide adjacent to the first damaged base, so that the damaged base was the first template site during primer extension. The positions of the primers and full-length products are indicated as 16 and 30, respectively. (B) The nucleotide incorporation profile was determined using an O^6-methyl-G template and one of the four dNTPs. The enzyme amounts of WT and L864F pol α were 180 and 13 ng, respectively. Other conditions are described in Section 2.

Table 4
Incorporation kinetics of WT and L864F pol α at O^6-MeG.

Enzyme	Template: dNTP	K_m (μM)	k_{cat} (min^{-1})	k_{cat}/K_m ($\mu M^{-1}\ min^{-1}$)	$f_{inc\text{-}1}$ [a]	$f_{inc\text{-}2}$ [b]
WT pol α	G:dCTP	1.4 ± 0.11	0.063 ± 0.011	0.044 ± 0.01	1	
	G:dTTP	310 ± 56	(2.7 ± 0.28) × 10^{-3}	(8.8 ± 0.70) × 10^{-6}	2.0 × 10^{-4}	
	O^6-MeG:dCTP	91 ± 7.8	0.013 ± 0.001	(1.5 ± 0.02) × 10^{-3}	0.034	1
	O^6-MeG:dTTP	19 ± 3.7	0.020 ± 0.002	(1.1 ± 0.14) × 10^{-3}	0.025	1
L864F pol α	dCTP	2.3 ± 0.33	0.072 ± 0.018	0.033 ± 0.009	1	
	dTTP	24 ± 1.3	0.053 ± 0.022	(2.2 ± 0.83) × 10^{-3}	0.067	
	O^6-MeG:dCTP	21 ± 3.9	0.17 ± 0.04	(8.3 ± 1.2) × 10^{-3}	0.25	7.4
	O^6-MeG:dTTP	12 ± 2.5	0.11 ± 0.040	0.010 ± 0.005	0.30	12

[a] Relative incorporation efficiency to $k_{cat}/K_{m(G:dCTP)}$.
[b] Relative incorporation efficiency to $f_{inc\text{-}1(O^6\text{-}MeG:dNTP,\ WT)}$.

Table 5
Extension kinetics of WT and L864F pol α at O^6-MeG.

Enzyme	Template: primer terminus	K_m (μM)	k_{cat} (min^{-1})	k_{cat}/K_m ($\mu M^{-1}\ min^{-1}$)	$f_{ext\text{-}1}$ [a]	$f_{ext\text{-}2}$ [b]
WT pol α	G:dC	4.6 ± 0.53	0.080 ± 0.020	0.018 ± 0.002	1	
	G:dT	110 ± 15	0.012 ± 0.0004	(1.2 ± 0.13) × 10^{-3}	0.006	
	O^6-MeG:dC	66 ± 12	0.021 ± 0.006	(3.2 ± 0.98) × 10^{-4}	0.018	1
	O^6-MeG:dT	160 ± 15	0.10 ± 0.049	(6.8 ± 3.5) × 10^{-4}	0.038	1
L864F pol α	G:dC	0.49 ± 0.09	0.17 ± 0.013	0.36 ± 0.04	1	
	G:dT	3.6 ± 0.84	0.17 ± 0.055	0.046 ± 0.009	0.13	
	O^6-MeG:dC	1.8 ± 0.16	0.31 ± 0.056	0.17 ± 0.044	0.47	26
	O^6-MeG:dT	1.5 ± 0.25	0.26 ± 0.001	0.18 ± 0.034	0.50	13

[a] Relative extension efficiency to $k_{cat}/K_{m(G:dC)}$.
[b] Relative extension efficiency to $f_{ext\text{-}1(O^6\text{-}MeG:dN,\ WT)}$.

which amplified a fragment involving the *POLA1*-plasmid junction region, as well as by restriction enzyme digestion using genomic DNA as a template (Fig. 4A and B). Expressions of plasmid-borne mRNAs and proteins were also examined by RT-PCR (Fig. 4C) and western blotting (Fig. 4D), respectively. These stable clones, which showed no apparent defect in cell growth (Fig. 4E), were used for determination of *HPRT* mutation rates (Section 2). As shown in Fig. 4F, HCT116 cells with *pola1L864F* (L864F pol α cells) had a mutation rate of 1.5×10^{-4}, which was twice as high as that of the wild-type (0.75×10^{-4}).

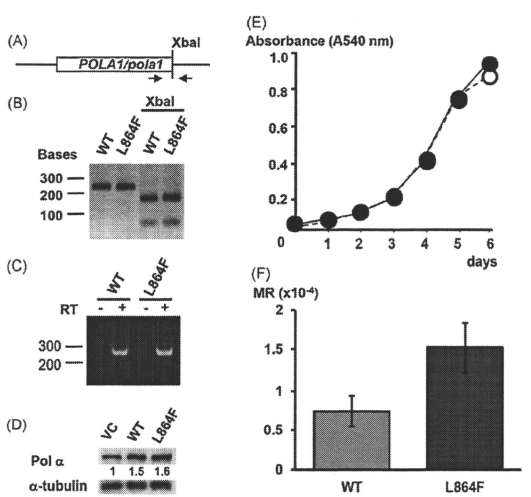

Fig. 4. Construction of stable clones with pol α expression and determination of mutation rate. (A) Schematic illustration of the *POLA1*/*pola1*-pcDNA3 junction. PCR primers and *XbaI* sites are shown. (B) PCR products were analyzed by agarose gel electrophoresis. Genomic DNA from HCT116 with wild-type (WT) or *pola1L864F* transfection (L864F) was used for a PCR template. The positions of the size markers are indicated on the left. In the right 2 lanes, *XbaI* was treated prior to gel electrophoresis. (C) cDNAs from stable cells were prepared and used for PCR templates (RT+). RT-refers to a mock experiment, in which cDNA preparation was carried out in the absence of reverse transcriptase (RT). (D) Western blotting analysis was carried out using an antibody against the pol α catalytic subunit. VC represents the vector control. α-Tubulin was used as a control. (E) Cell growth of WT (filled circles) and L864F (open circles) was determined by MTT assays and plotted. (F) Mutation rates (MR) of HCT116 cells with WT or L864F pol α transfection were determinded as described in Section 2. Ranges of confidence limits are also shown.

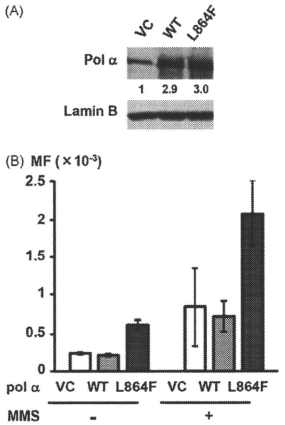

Fig. 5. Transient pol α expression and determination of mutant frequency. (A) Overexpression of wild-type (WT) or L864F pol α (L864F) was monitored, then quantified and compared with the vector control (VC) using western blotting. (B) Lamin B was used as a control. Both spontaneous and MMS-induced mutant frequencies (MF) were determined as described in Section 2, and presented as a graph with the values shown as the average ± SD (5 independent experiments).

3.4. Transient pol α overexpression

During the cloning process of HCT116 clones, we noticed that pol α expression rapidly decreased to nearly the basal level. To analyze *HPRT* mutations with high expression levels of exogenous pol α, we used a transient overexpression system, in which the expression levels of wild-type and L864F pol α were 3.4- and 3.6-fold higher than that of vector-control cells (Fig. 5). We found that cells with transient overexpression of the wild-type pol α showed a mutant frequency of 2.4×10^{-4}, which approximated that of the vector control (2.8×10^{-4}). On the other hand, L864F pol α showed a mutant frequency of 7.1×10^{-4}, which were 2.6- and 2.9-fold higher than those of the vector control and wild-type pol α, respectively. These results suggest that L864F pol α performs error-prone DNA replication in HCT116 cells.

We also treated cells with MMS prior to the *HPRT* mutation assays. Mutant frequencies of both the vector control and wild-type pol α cells were increased to 0.84×10^{-3} and 0.72×10^{-3}, respectively, which were roughly 3-fold higher than under spontaneous conditions. If L864F pol α performs error-prone translesion DNA synthesis in HCT116 cells, then the mutant frequency of L864F pol α cells would also be higher than that of the wild-type. If not, the differences in minor spontaneous mutation frequencies would be buried in the induced mutation frequencies. Our results showed that the mutant frequency of L864F pol α cells was 2.1×10^{-3}, which was 2.9-fold higher than that of the wild-type pol α cells, suggesting that error-prone translesion DNA synthesis also occurred in HCT116.

4. Discussion

To date, little has been reported regarding the significance of the base selection step in human DNA polymerases, though it has been well analyzed in *S. cerevisiae* and prokaryotes ([2,26] and references therein). To study this in human cells, we used L864F pol α, because pol α intrinsically lacks 3′–5′ exonuclease activity and provided the simplest experimental system. Furthermore, studies of *S. cerevisiae* have shown that the mutation rate with the corresponding *pol1L868F* allele was increased to a level comparable to that of the mutator pol δ and ε strains of *pol2* and *pol3*, respectively [7,21].

Before we introduced the mutator pol α into the cell lines, we characterized the biochemical properties of L864F pol α. In M13mp2 forward mutation and kinetic analyses, L864F pol α was found to be a mutator pol with normal template DNA (Tables 1–3 and Fig. 2). HCT116 cells with L864F pol α transfection had increased numbers of *HPRT* mutations as compared to those transfected with the wild-type (Figs. 4 and 5). Furthermore, L864F pol α replicated DNA over types of alkylated DNA damages with relative ease (Fig. 3). Results of our kinetic analyses showed that L864F pol α efficiently promoted dCMP and dTMP incorporation and extension at the O^6-methyl-G site (Tables 4 and 5, $f_{inc\text{-}2}$). This performance may have increased the translesion efficiency and mutation frequency, when such DNA lesions existed in DNA and L864F pol α was overexpressed in HCT116 cells (Fig. 5B). Based on these results, we concluded that L864F pol α has an increased level of spontaneous mutation frequency by incorporating the wrong nucleotides in the normal template and translesion DNA synthesis at some endogenously damaged sites.

We performed cellular mutation assays under the condition of exogenous expression of wild-type or L864F pol α. Overexpression of wild-type pol α did not alter the mutant frequency from that of the vector control in HCT116 cells (Fig. 5), thus this strategy allowed us to compare mutagenic phenotypes between wild-type and L864F pol α. In assays using stable clones, we observed only modest overexpression, as indicated by western blotting findings (Fig. 4D). Therefore, a small amount of L864F pol α may have been expressed and the mutation rates might be underestimated. In transient assays, under conditions where exogenous pol α was expressed a few fold higher than endogenous levels, we obtained very similar results to those obtained with stable clones. We do not deny the possibility that overexpressed wild-type or L864F pol α was inappropriately used during Okazaki fragment synthesis in both experiments. For example, pol α could be used for DNA replication more frequently than it is under the physiological expression level. In either case, we must wait for future experiments using knock-in mice or other gene targeting systems.

Because the fidelity of pol α is lower than that of processive replicative pols, DNA replication errors may occur relatively frequently near the 5′ ends of the Okazaki fragments and DNA replication origins. In fact, a high rate of pol α errors was previously observed at the *trp1/ARS1* locus in *pol1L868F* [7]. Regarding the error-processing pathway for pol α, previous studies have proposed that the errors are removed by FEN1 during Okazaki fragment maturation [27] or are proofread by pol δ [25]. It has also been shown that generation of pol α-dependent +1 frameshifts depends on pol ζ functions [21]. For future study of these transacting pathways in human cells, introduction of error-prone pols may provide an effective approach to assess putative error prevention as well as error promotion pathways that underlie genomic instability and cancer.

Conflict of interest

None.

Acknowledgements

We thank Drs. Hiro-o Ishihara, Kiyoshi Yanagisawa, and Tomoya Yamaguchi for their critical discussion. We are also grateful for the generous assistance of Sachiko Takahashi and Kumiko Kobayashi. This work was supported in part by a Grant-in-Aid for Scien-

tific Research on Innovative Areas, a Grant-in-Aid for Scientific Research on Priority Areas from the Ministry of Education, Culture, Sports, Science, and Technology of Japan, a Grant-in-Aid for Scientific Research from the Japan Society for the Promotion of Science, the Aichi Cancer Research Foundation, and the Novartis Foundation (Japan) for the Promotion of Science.

References

[1] Y.I. Pavlov, P.V. Shcherbakova, I.B. Rogozin, Int. Rev. Cytol. 255 (2006) 41–132.
[2] S.D. McCulloch, T.A. Kunkel, Cell Res. 18 (2008) 148–161.
[3] P.H. Patel, H. Kawate, E. Adman, M. Ashbach, L.A. Loeb, J. Biol. Chem. 276 (2001) 5044–5051.
[4] M. Suzuki, A.K. Avicola, L. Hood, L.A. Loeb, J. Biol. Chem. 272 (1997) 11228–11235.
[5] M. Suzuki, S. Yoshida, E.T. Adman, A. Blank, L.A. Loeb, J. Biol. Chem. 275 (2000) 32728–32735.
[6] L.J. Reha-Krantz, R.L. Nonay, J. Biol. Chem. 269 (1994) 5635–5643.
[7] A. Niimi, S. Limsirichaikul, S. Yoshida, S. Iwai, C. Masutani, F. Hanaoka, E.T. Kool, Y. Nishiyama, M. Suzuki, Mol. Cell. Biol. 24 (2004) 2734–2746.
[8] Z.F. Pursell, I. Isoz, E.B. Lundstrom, E. Johansson, T.A. Kunkel, Science 317 (2007) 127–130.
[9] L. Li, K.M. Murphy, U. Kanevets, L.J. Reha-Krantz, Genetics 170 (2005) 569–580.
[10] R.N. Venkatesan, J.J. Hsu, N.A. Lawrence, B.D. Preston, L.A. Loeb, J. Biol. Chem. 281 (2006) 4486–4494.
[11] J. Jiricny, Nat. Rev. Mol. Cell. Biol. 7 (2006) 335–346.
[12] R.E. Goldsby, L.E. Hays, X. Chen, E.A. Olmsted, W.B. Slayton, G.J. Spangrude, B.D. Preston, Proc. Natl. Acad. Sci. U.S.A. 99 (2002) 15560–15565.
[13] R.E. Goldsby, N.A. Lawrence, L.E. Hays, E.A. Olmsted, X. Chen, M. Singh, B.D. Preston, Nat. Med. 7 (2001) 638–639.
[14] M. Simon, L. Giot, G. Faye, EMBO J. 10 (1991) 2165–2170.
[15] R.N. Venkatesan, P.M. Treuting, E.D. Fuller, R.E. Goldsby, T.H. Norwood, T.A. Gooley, W.C. Ladiges, B.D. Preston, L.A. Loeb, Mol. Cell. Biol. 27 (2007) 7669–7682.
[16] A. Morrison, J.B. Bell, T.A. Kunkel, A. Sugino, Proc. Natl. Acad. Sci. U.S.A. 88 (1991) 9473–9477.
[17] M. Takemura, K. Sugimura, K. Okumura, S. Limsirichaikul, M. Suzuki, Y. Yamada, S. Yoshida, Biosci. Biotechnol. Biochem. 72 (2008) 630–635.
[18] S. Limsirichaikul, M. Ogawa, A. Niimi, S. Iwai, T. Murate, S. Yoshida, M. Suzuki, J. Biol. Chem. 278 (2003) 19079–19086.
[19] M. Ogawa, S. Limsirichaikul, A. Niimi, S. Iwai, S. Yoshida, M. Suzuki, J. Biol. Chem. 278 (2003) 19071–19078.
[20] H. Matsubara, T. Takeuchi, E. Nishikawa, K. Yanagisawa, Y. Hayashita, H. Ebi, H. Yamada, M. Suzuki, M. Nagino, Y. Nimura, H. Osada, T. Takahashi, Oncogene 26 (2007) 6099–6105.
[21] M. Suzuki, A. Niimi, S. Limsirichaikul, S. Tomida, Q.M. Huang, S. Izuta, J. Usukura, Y. Itoh, T. Hishida, T. Akashi, Y. Nakagawa, A. Kikuchi, Y. Pavlov, T. Murate, T. Takahashi, J. Biochem. 146 (2009) 13–21.
[22] X. Zhong, L.C. Pedersen, T.A. Kunkel, Nucleic Acids Res. 36 (2008) 3892–3904.
[23] J.Y. Choi, G. Chowdhury, H. Zang, K.C. Angel, C.C. Vu, L.A. Peterson, F.P. Guengerich, J. Biol. Chem. 281 (2006) 38244–38256.
[24] L.J. Reha-Krantz, R.L. Nonay, R.S. Day, S.H. Wilson, J. Biol. Chem. 271 (1996) 20088–20095.
[25] Y.I. Pavlov, C. Frahm, S.A. Nick McElhinny, A. Niimi, M. Suzuki, T.A. Kunkel, Curr. Biol. 16 (2006) 202–207.
[26] P.H. Patel, M. Suzuki, E. Adman, A. Shinkai, L.A. Loeb, J. Mol. Biol. 308 (2001) 823–837.
[27] J.A. Rumbaugh, L.A. Henricksen, M.S. DeMott, R.A. Bambara, J. Biol. Chem. 274 (1999) 14602–14608.

Biochemical and Biophysical Research Communications 391 (2010) 542–546

Contents lists available at ScienceDirect

Biochemical and Biophysical Research Communications

journal homepage: www.elsevier.com/locate/ybbrc

Roles of POLD4, smallest subunit of DNA polymerase δ, in nuclear structures and genomic stability of human cells

Qin Miao Huang [a], Tomohiro Akashi [b], Yuji Masuda [c], Kenji Kamiya [c], Takashi Takahashi [a], Motoshi Suzuki [a,*]

[a] Division of Molecular Carcinogenesis, Center for Neurological Diseases and Cancer, Nagoya University Graduate School of Medicine, Nagoya, Japan
[b] Division of Molecular Mycology and Medicine, Center for Neurological Diseases and Cancer, Nagoya University Graduate School of Medicine, Nagoya, Japan
[c] Research Institute for Radiation Biology and Medicine, Hiroshima University, Hiroshima 734-8553, Japan

ARTICLE INFO

Article history:
Received 13 November 2009
Available online 24 November 2009

Keywords:
POLD4
Karyomere
Micronuclei
Cell cycle
DNA replication
DNA damage

ABSTRACT

Mammalian DNA polymerase δ (pol δ) is essential for DNA replication, though the functions of this smallest subunit of POLD4 have been elusive. We investigated pol δ activities *in vitro* and found that it was less active in the absence of POLD4, irrespective of the presence of the accessory protein PCNA. shRNA-mediated reduction of POLD4 resulted in a marked decrease in colony formation activity by Calu6, ACC-LC-319, and PC-10 cells. We also found that POLD4 reduction was associated with an increased population of karyomere-like cells, which may be an indication of DNA replication stress and/or DNA damage. The karyomere-like cells retained an ability to progress through the cell cycle, suggesting that POLD4 reduction induces modest genomic instability, while allowing cells to grow until DNA damage reaches an intolerant level. Our results indicate that POLD4 is required for the *in vitro* pol δ activity, and that it functions in cell proliferation and maintenance of genomic stability of human cells.

Introduction

Eukaryotic DNA polymerase δ (pol δ), a key enzyme that participates in DNA replication and repair, consists of four subunits; POLD1 (catalytic subunit, alternatively called p125), POLD2 (p50), POLD3 (p68), and POLD4 (p12) [1,2]. Among those, POLD4 binds to POLD1, POLD2, and an accessory protein of PCNA, which allows pol δ to exhibit its full activity [1,3].

A previous study showed that the *POLD4* ortholog of *Cdm1* in *Schizosaccharomyces pombe* is a non-essential gene related to cell growth, division, and sensitivity to DNA damaging reagents [4]. *Saccharomyces cerevisiae* does not have a POLD4 counterpart, indicating that POLD4 is dispensable in lower eukaryotic cells. In contrast, siRNA-mediated knockdown of POLD4 caused a significant decrease in the proliferation rate of FGF2-activated mouse-endothelial cells [5]. However, it remains unknown whether POLD4 is required for other types of mammalian cells, such as those related to human cancer, or if it has additional functions in mammalian cells.

In the present study, we analyzed the roles of POLD4 for cell proliferation in human lung cancer cell lines. Our findings indicate that POLD4 is required for maintaining the proper nuclear structures and suggest that the pathological structures reflect elevated DNA damage in chromosomes.

* Corresponding author. Address: Division of Molecular Carcinogenesis, Center for Neurological Diseases and Cancer, Nagoya University Graduate School of Medicine, Nagoya 466-8550, Japan.
E-mail address: msuzuki@med.nagoya-u.ac.jp (M. Suzuki).

0006-291X/$ - see front matter © 2009 Elsevier Inc. All rights reserved.
doi:10.1016/j.bbrc.2009.11.094

Materials and methods

Antibodies. The antibodies used in this study were anti-POLD4 (POLD4 subunit of pol δ) ascites (2B11, Abnova, Taipei City, Taiwan), anti-lamin B (c-20) (Santa Cruz Biotechnology, Santa Cruz, CA), and anti-γ-tubulin (Sigma–Aldrich, St. Louis, MO).

In vitro pol δ activity. Three- and 4-subunit DNA from pol δ were expressed in *Escherichia coli*, and purified as described previously [6]. pol δ activity was determined in a reaction mixture (25 μl) containing 20 mM HEPES–NaOH (pH 7.5), 50 mM NaCl, 0.2 mg/ml BSA, 1 mM dithiothreitol, 10 mM $MgCl_2$, 1 mM ATP, 0.1 mM each of dGTP, dATP, dCTP, and [α-^{32}P]dTTP, 100 ng poly dA-oligo dT (GE Healthcare, Piscataway, NJ), 86 ng (1.0 pmol as a trimer) of PCNA, and 11–88 ng (46–372 fmol) of pol δ at 30 °C for 10 min. Following incubation, the reactions were terminated with 2 μl of 300 mM EDTA. pol activity was determined with reference to the incorporation of [α-^{32}P]dTMP, as previously described [6].

Colony formation assay. To assess cell proliferation, colony formation assays were performed as previously described [7]. In order to rule out the off-target effect, we designed two independent DNA sequences as follows: MS543F, 5′-GATCCCCagtctctggcatctctatcATTCAAGAGATgatagagatgccagagactTTTTTGGAAA-3; MS544R, 5′-AGCTTTTCCAAAAAagtctctggcatctctatcATCTCTTGAATgatagagatgccagagactGGG-3; MS551F, 5′-GATCCCCgcatctctatccccatgaATTCAAGAGATtcataggggatagagatgcTTTTTGGAAA-3; and MS552R, 5′-AGCTTTTCCAAAAAgcatctctatcccctatgaATCTCTTGAATtcataggggatagagatgcGGG-3, in which the targeting sequences are indicated in lowercase letters. To construct shRNA vectors, MS543F and MS544R

(polD4-5), and MS551F and MS552R (polD4-3-1) were annealed, then inserted between the restriction sites BglII and HindIII in PH1RNAneo [7]. Cells transfected with a vector carrying either polD4-3-1 or polD4-5 were cultured in media containing 1 mg/ml G418 (Invitrogen, Carlsbad, CA 10131-027), which was reduced by 0.2 mg/ml every 2 days until it reached 0.4 mg/ml. When colonies grew to visible seizes, they were fixed by cold methanol for 5 min and stained with 4% Giemsa for 15 min at room temperature.

RNA interference. Transfection was carried out using 50 nmol/L of a small interfering RNA (siRNA) duplex (Sigma–Aldrich) targeting each mRNA, or negative control 1# (Ambion) with Lipofectamine-2000 (Invitrogen). The sequences of si*POLD4* were the same as those of polD4-3-1: *POLD4* (si*D4*) sense, 5′-GCAUCUCUAUCCCCUAUGATT-3′; and antisense, 5′-UCAUAGGGGAUAGAGAUGCTT.

Laser scanning cytometry (LSC). Following an overnight culture, 3×10^5/ml Calu6 cells on coverslips were fixed by cold methanol, washed with PBS, and incubated with 1 mg/ml RNase A in 50 mM Tris–HCl, pH 7.5, at 37 °C for 1 h. Cells were further treated with 50 μg/ml propidium iodide in a mixture containing 180 mM Tris–HCl, pH 7.5, 180 mM NaCl, and 70 mM $MgCl_2$ for 15 min. Nuclei structures and DNA contents were analyzed using a Laser Scanning Cytometer (LSC, Olympus, Tokyo, Japan), with DNA content at the G1 peak regarded as 2N, though Calu6 cells carry a greater amount of DNA chromatin than normal cells.

Cell cycle synchronization. Calu6 cells were synchronized according to the method of Nakagawa et al. [8], with minor modifications. In brief, 24-h treatment with 2 mM thymidine was used to arrest exponentially proliferating cells in the S phase. Cells were then released from arrest by three washes in PBS and grown in fresh medium for 15 h, then 1 μM of aphidicolin was used for the second block for 10 h. After releasing by three washes in PBS, cells were incubated in RPMI1640 containing 5% fetal bovine serum and harvested at various time points.

Immunofluorescence. Following an overnight culture, 3×10^5/ml Calu6 cells on coverslips were transfected with siRNA as described above. After 48 h, they were fixed in 4% paraformaldehyde for 10 min at room temperature, followed by treatment with cold methanol for 2 min. The coverslips were washed three times in PBS, treated with PBS containing 0.25% Triton X-100 on ice for 30 min, and incubated with anti-lamin B or anti-γ-tubulin antibody overnight at 4 °C. The cells were then washed three times in PBS, incubated for 1 h with Alexa 488-conjugated secondary antibody (Molecular Probes, OR, USA), and analyzed using an Olympus BX60 (Olympus).

Results and discussion

DNA synthesis activities of pol δ with or without POLD4 in vitro

In order to analyze POLD4 functions related to intrinsic pol δ activity, 3- and 4-subunit structures of pol δ were expressed and purified. In the absence of POLD4, pol δ was less active than the holoenzyme in a reaction containing poly dA–dT as a template primer (Fig. 1A), with a similar result obtained when the accessory protein of PCNA was omitted from the reaction (Fig. 1B). These results are consistent with those of previous studies [1,3] and indicate that POLD4 is required for pol δ to exhibit its full catalytic activity.

POLD4 required for cell proliferation

A previous genetic study of *S. pombe* demonstrated that the *POLD4* ortholog of *Cdm1* is a non-essential gene for cell growth,

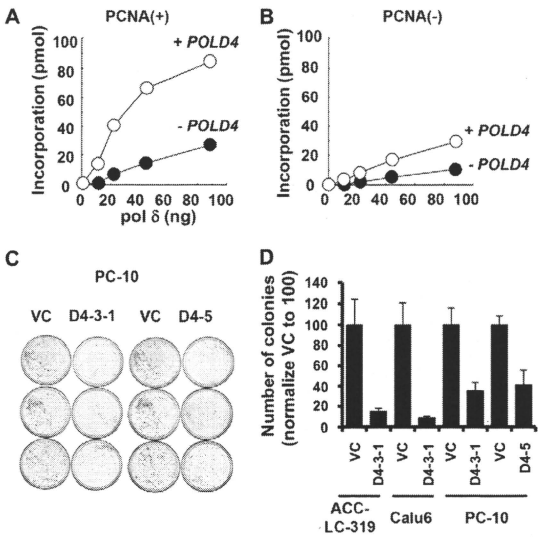

Fig. 1. *In vitro* DNA synthesis activities of pol δ and effect of POLD4 depletion on colony formation activity. (A) pol δ activities were measured and plotted as described in Materials and methods. (B) The same reactions were carried out in the absence of PCNA. (C) PC-10 was used for transfection with plasmids carrying either D4-3-1 or D4-5, and colony formation activity was determined as described in Materials and methods. VC represents vector control. (D) Results of the colony formation assay were plotted in a graph.

division, and sensitivity to DNA damaging reagents [4]. Nevertheless, it is possible that mammalian cells with larger genomic sizes require POLD4 for efficient and accurate DNA replication. We investigated this possibility using shRNA-mediated knockdown of *POLD4*. As shown in Fig. 1C, two independent sequences of shRNA caused reduced activity in a colony formation assay using PC-10, a human non-small cell lung cancer (NSCLC) cell line. Similar results were obtained with different NSCLC cell lines, Calu6 and ACC-LC-319 (Fig. 1D). These findings suggest that human cells require POLD4 for proliferation.

Structure and population of karyomere-like cells following siPOLD4 treatment

Since pol δ is a major DNA replication and repair polymerase, impairment of its activity may cause DNA replication stress, such as accumulation of single-stranded DNA gaps, and inefficient repair of endogenous DNA damage, which ultimately results in cell death. On the other hand, it is also possible that some cells continue to grow following such genetic erosion, which may cause genomic instability. Therefore, we investigated whether POLD4 is also required for suppressing genomic instability in human cells. Initially, we attempted to establish stable clones with low POLD4 expression using shRNA-treated cells. However, clones with adequate levels of POLD4 expression were gradually selected, leading to recovery to the original level over time (data not shown). Therefore, in the following experiments, we used siRNA to transiently reduce POLD4 expression (Fig. 2A, left).

Calu6 cells treated with si*POLD4* formed multiple or lobed nuclei, at a 5.3-fold greater frequency than in the control experiment (Fig. 2B and C). Similar structures were also observed when A549 cells were treated with si*POLD4* (data not shown). Staining with

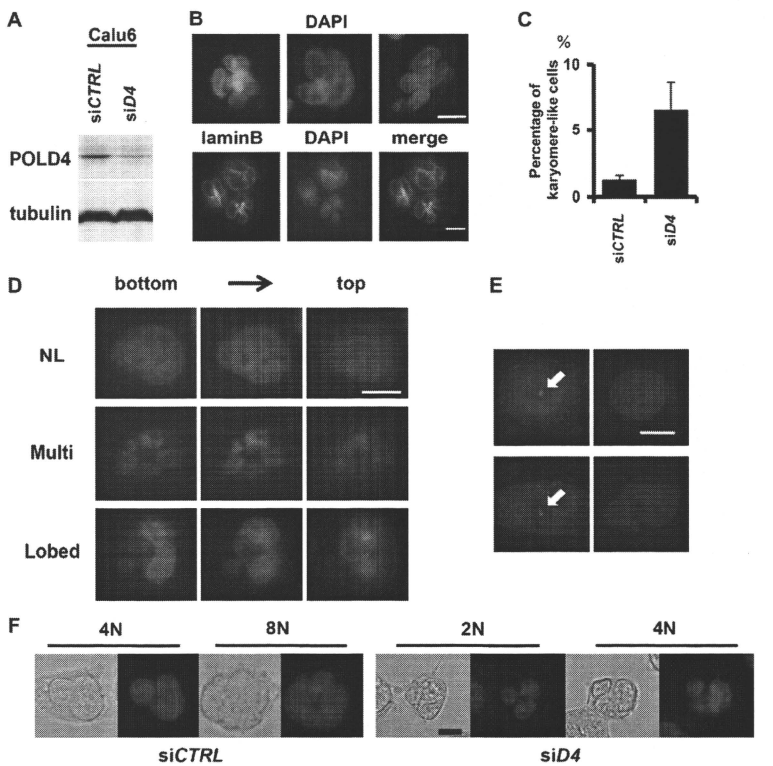

Fig. 2. Structures and population of karyomere-like cells upon si*POLD4* treatment. (A) Western blot analysis of POLD4 and α-tubulin in protein extracts from si*POLD4*- or si*CTRL*-treated Calu6 cells. (B) Upper panels: Calu6 cells were treated with si*POLD4* for 48 h and stained with DAPI. Sample karyomere-like nuclei are shown. Lower panels: Calu6 cells were treated with si*POLD4* for 48 h, then visualized with anti-lamin B antibody or DAPI. (C) Calu6 cells were treated with si*POLD4* or si*CTRL*, then the frequencies of karyomere-like structures in 1000 cells were counted and plotted. In this experiment, cells with three or more nuclear lobes, or three or more nuclei were regarded as karyomere-like cells. Averages of three independent results are shown with SD. (D) si*POLD4*-treated cells were stained by DAPI, then three sequential photographs were taken every 4 μm from the bottom. Upper, middle, and lower panels show images of normal, multiple, and lobed nuclear structures, respectively. (E) After being treated with si*POLD4*, cells were visualized with anti-γ-tubulin (left) or DAPI (right). Upper and lower panels show representative pictures of normal and karyomere-like nuclei, respectively. Centrosomes are indicated by arrows. (F) LSC analysis. Phase-contrast and propidium iodide-stained images of karyomere-like cells among 4N and 8N (si*CTRL*), or 2N and 4N (si*POLD4*) cells. Bar indicates 10 μm.

the anti-lamin B antibody outlined the edges of the DAPI structures and showed that the nuclear envelope was formed around chromatin (Fig. 2B, lower). Sequential acquisition of images from the bottom of the cells further illustrated the abnormal structures of single cells, including a flat profile and multiple nuclei (Fig. 2D, middle panels), or a single nucleus associated with multiple lobes (Fig. 2D, lower panels). For both types of abnormal structures, the nuclear sizes were approximately that of a normally shaped nucleus (Fig. 2D, upper panels).

The multiple nuclei seen with these structures were reminiscent of 'micronuclei' that indicated the presence of DNA damage and DNA replication stress in previous studies [9–11], while the lobed nuclei closely resembled 'karyomere' nuclei observed in zebrafish blastomeres [12] and early *Xenopus laevis* development [13]. In that latter study and other studies referenced therein, it was suggested that karyomere formation is a physiological mitotic process that may share similar mechanisms with pathological micronuclei formation; with both multiple and lobed nuclei, isolated chromosomes might

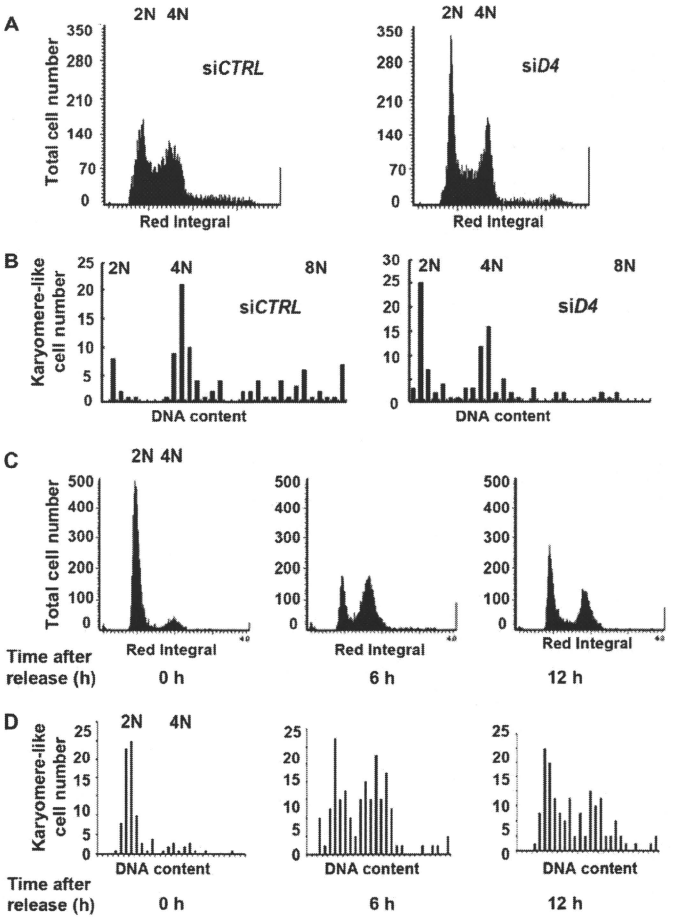

Fig. 3. Cell cycle dynamics of karyomere-like cells. (A) Calu6 cells were treated with si*CTRL* (left) or si*POLD4* (right), then their DNA contents were subjected to LSC analysis. The G1 population found among the majority of cells was regarded as 2N. (B) In the same experiment, DNA contents of 100 karyomere-like cells were determined. Cell numbers in each DNA content range were plotted with histograms. (C) Calu6 cells were treated with si*POLD4*, then synchronized at the G1/S boundary and released for cell cycle progression. At 0, 6, or 12 h after release, DNA contents were subjected to LSC. (D) In the same experiment, the DNA contents of 100 karyomere-like cells were measured. Cell numbers in each DNA content range were plotted with histograms.

be surrounded by a nuclear envelope after chromosome segregation occurs. Therefore, those two types of abnormal structures are referred to as karyomere-like nuclei hereafter.

In addition to DNA damage, formation of karyomere-like nuclei may also occur as a consequence of dysfunctions of the mitotic apparatus [13,14]. Moreover, a previous study found that the anti-POLD4 antibody bound the surface of mitotic chromosomes, which suggests specific functions of POLD4 during mitosis [5]. To investigate this, we analyzed the centrosome structures in si *POLD4*-treated cells, as it has been reported that disturbed chromosomal migration occurred with abnormal replication or localization of centrosomes [15,16]. Our present results showed that si *POLD4*-treated cells were associated with normal centrosome structures, which had one or two centrosomes located at a single site (Fig. 2E). We also quantified the lagging-chromosome frequencies, and found that they were very similar between si*POLD4*- and si*CTRL*-treated mitotic cells (data not shown). Although the results of this limited experiment were contrary to our speculation that POLD4 has some mitotic functions, we intend to conduct more detailed examinations in the future.

Cell cycle dynamics of karyomere-like cells

In the following experiments, we studied the cell cycle dynamics of karyomere-like cells. After si*POLD4* treatment, we observed checkpoint activation (data not shown, detailed mechanisms discussed elsewhere), and accumulations of G1- and G2-populations (Fig. 3A). In si*CTRL*-treated cells, most of the karyomere-like populations were found among the minor aneuploid populations (Figs. 3B and 2F, left panels). In contrast, karyomere-like cells in si *POLD4*-treated cells were found to have normal ploidy as seen with 2N–4N cells (Fig. 3B, 2F, right panels).

In order to determine if karyomere-like cells remained alive and had an ability to progress through the cell cycle, we synchronized cells at the G1–S boundary, then released them and observed the cell cycle progression, as well as the associated nuclear shapes (Fig. 3C–E). Interestingly, karyomere-like cells progressed through the cell cycle and returned to G1 at 12 h after release. In support of these results, most karyomere-like cells were negative in TUNEL staining findings (data not shown). Therefore, these structures may not reflect the pro-apoptotic phenotype. Our results suggest that most karyomere-like cells are able to proliferate until they became arrested at the G1 or G2 phase, when DNA damage reaches an intolerant level.

In conclusion, our results showed that POLD4 supports cellular proliferation and suppresses karyomere-like nuclei formation in human cells, which might occur as a consequence of impairment of the DNA replication and repair activities of pol δ. A future study to identify the direct link between POLD4 and mitotic functions may reveal the underlying mechanisms to maintain genomic stability in human cells.

Acknowledgments

We thank Keiko Ueda and Makiko Terada for their initial involvement in this project. We are also grateful for Dr. Takeshi Senga of our university for the critical reading of the manuscript. This work was supported in part by a Grant-in-Aid for Scientific Research on Innovative Areas, a Grant-in-Aid for Scientific Research on Priority Areas from the Ministry of Education, Culture, Sports, Science, and Technology of Japan, and a Grant-in-Aid for Scientific Research from the Japan Society for the Promotion of Science.

References

[1] V.N. Podust, L.S. Chang, R. Ott, G.L. Dianov, E. Fanning, Reconstitution of human DNA polymerase delta using recombinant baculoviruses: the p12 subunit potentiates DNA polymerizing activity of the four-subunit enzyme, J. Biol. Chem. 277 (2002) 3894–3901.

[2] L. Liu, J. Mo, E.M. Rodriguez-Belmonte, M.Y. Lee, Identification of a fourth subunit of mammalian DNA polymerase delta, J. Biol. Chem. 275 (2000) 18739–18744.

[3] H. Li, B. Xie, Y. Zhou, A. Rahmeh, S. Trusa, S. Zhang, Y. Gao, E.Y. Lee, M.Y. Lee, Functional roles of p12, the fourth subunit of human DNA polymerase delta, J. Biol. Chem. 281 (2006) 14748–14755.

[4] N. Reynolds, A. Watt, P.A. Fantes, S.A. MacNeill, Cdm1, the smallest subunit of DNA polymerase d in the fission yeast *Schizosaccharomyces pombe*, is non-essential for growth and division, Curr. Genet. 34 (1998) 250–258.

[5] P. Dell'Era, S. Nicoli, G. Peri, M. Nieddu, M.G. Ennas, M. Presta, FGF2-induced upregulation of DNA polymerase-delta p12 subunit in endothelial cells, Oncogene 24 (2005) 1117–1121.

[6] Y. Masuda, M. Suzuki, J. Piao, Y. Gu, T. Tsurimoto, K. Kamiya, Dynamics of human replication factors in the elongation phase of DNA replication, Nucleic Acids Res. 35 (2007) 6904–6916.

[7] H. Tanaka, K. Yanagisawa, K. Shinjo, A. Taguchi, K. Maeno, S. Tomida, Y. Shimada, H. Osada, T. Kosaka, H. Matsubara, T. Mitsudomi, Y. Sekido, M. Tanimoto, Y. Yatabe, T. Takahashi, Lineage-specific dependency of lung adenocarcinomas on the lung development regulator TTF-1, Cancer Res. 67 (2007) 6007–6011.

[8] T. Nakagawa, Y. Hayashita, K. Maeno, A. Masuda, N. Sugito, H. Osada, K. Yanagisawa, H. Ebi, K. Shimokata, T. Takahashi, Identification of decatenation G2 checkpoint impairment independently of DNA damage G2 checkpoint in human lung cancer cell lines, Cancer Res. 64 (2004) 4826–4832.

[9] N. Holland, C. Bolognesi, M. Kirsch-Volders, S. Bonassi, E. Zeiger, S. Knasmueller, M. Fenech, The micronucleus assay in human buccal cells as a tool for biomonitoring DNA damage: the HUMN project perspective on current status and knowledge gaps, Mutat. Res. 659 (2008) 93–108.

[10] J.B. Bae, S.S. Mukhopadhyay, L. Liu, N. Zhang, J. Tan, S. Akhter, X. Liu, X. Shen, L. Li, R.J. Legerski, Snm1B/Apollo mediates replication fork collapse and S phase checkpoint activation in response to DNA interstrand cross-links, Oncogene 27 (2008) 5045–5056.

[11] D.J. Kirkland, L. Henderson, D. Marzin, L. Muller, J.M. Parry, G. Speit, D.J. Tweats, G.M. Williams, Testing strategies in mutagenicity and genetic toxicology: an appraisal of the guidelines of the European Scientific Committee for Cosmetics and Non-Food Products for the evaluation of hair dyes, Mutat. Res. 588 (2005) 88–105.

[12] V.K. Schoft, A.J. Beauvais, C. Lang, A. Gajewski, K. Prufert, C. Winkler, M.A. Akimenko, M. Paulin-Levasseur, G. Krohne, The lamina-associated polypeptide 2 (LAP2) isoforms beta, gamma and omega of zebrafish: developmental expression and behavior during the cell cycle, J. Cell Sci. 116 (2003) 2505–2517.

[13] J.M. Lemaitre, G. Geraud, M. Mechali, Dynamics of the genome during early *Xenopus laevis* development: karyomeres as independent units of replication, J. Cell Biol. 142 (1998) 1159–1166.

[14] M. Ohsugi, K. Adachi, R. Horai, S. Kakuta, K. Sudo, H. Kotaki, N. Tokai-Nishizumi, H. Sagara, Y. Iwakura, T. Yamamoto, Kid-mediated chromosome compaction ensures proper nuclear envelope formation, Cell 132 (2008) 771–782.

[15] D. Eriksson, P.O. Lofroth, L. Johansson, K.A. Riklund, T. Stigbrand, Cell cycle disturbances and mitotic catastrophes in HeLa Hep2 cells following 2.5 to 10 Gy of ionizing radiation, Clin. Cancer Res. 13 (2007) 5501s–5508s.

[16] H. Dodson, E. Bourke, L.J. Jeffers, P. Vagnarelli, E. Sonoda, S. Takeda, W.C. Earnshaw, A. Merdes, C. Morrison, Centrosome amplification induced by DNA damage occurs during a prolonged G2 phase and involves ATM, EMBO J. 23 (2004) 3864–3873.

nature genetics

Variation in *TP63* is associated with lung adenocarcinoma susceptibility in Japanese and Korean populations

Daiki Miki[1,2], Michiaki Kubo[3], Atsushi Takahashi[4], Kyong-Ah Yoon[5], Jeongseon Kim[5], Geon Kook Lee[5], Jae Ill Zo[5], Jin Soo Lee[5], Naoya Hosono[3], Takashi Morizono[6], Tatsuhiko Tsunoda[6], Naoyuki Kamatani[4], Kazuaki Chayama[2], Takashi Takahashi[7], Johji Inazawa[8], Yusuke Nakamura[1] & Yataro Daigo[1,9,10]

Lung cancer is the most common cause of death from cancer worldwide, and its incidence is increasing in East Asian and Western countries. To identify genetic factors that modify the risk of lung adenocarcinoma, we conducted a genome-wide association study in a Japanese cohort, with replication in two independent studies in Japanese and Korean individuals, in a total of 2,098 lung adenocarcinoma cases and 11,048 controls. The combined analyses identified two susceptibility loci for lung adenocarcinoma: *TERT* (rs2736100, combined $P = 2.91 \times 10^{-11}$, odds ratio (OR) = 1.27) and *TP63* (rs10937405, combined $P = 7.26 \times 10^{-12}$, OR = 1.31). Fine mapping of the region containing *TP63* showed that a SNP (rs4488809) in intron 1 of *TP63* showed the most significant association. Our results suggest that genetic variation in *TP63* may influence susceptibility to lung adenocarcinoma in East Asian populations.

Primary lung cancer is a leading cause of death from cancer in most countries[1,2]. Lung cancer comprises various types of histology that are often divided into two main types, non–small-cell lung cancer and small-cell lung cancer. Each type has different pathophysiological and clinical features, suggesting that their mechanisms of carcinogenesis differ[3]. Adenocarcinoma accounts for about 50% of all histological types of lung cancer, and its incidence is increasing in East Asian and Western countries[4–14].

Previous studies have suggested that inherited genetic factors have a significant role in lung cancer development[15,16]. Genome-wide association studies (GWAS) of lung cancer in populations of European ancestry have identified the 15q24–25.1 region to be the most significantly associated region; this region contains genes that encode nicotinic acetylcholine receptor subunits (*CHRNA5*, *CHRNA3* and *CHRNA4*)[17–22]. Other GWAS of lung cancer identified two associated risk loci at 5p15.33 (*TERT-CLPTM1L*) and 6p21.33 (*BAT3-MSH5*)[20–22]. These signals at 5p15, 6p21 and 15q25 have been refined in European populations by a GWAS that searched for inherited susceptibility to specific histological types of lung cancer. In this GWAS meta-analysis, rs2736100 (in *TERT*) was indicated to be associated with risk of lung adenocarcinoma, and no additional loci were shown to reach genome-wide significance[23]. Because most of the current GWAS on lung cancer have been conducted in European populations with a full range of different histological types of lung cancer, GWAS that focus on individual histological groups with archived clinicopathological features are required. The allelic frequencies of the strong susceptibility locus at 15q25 in European populations are very rare in Asian populations. The risk-associated SNPs in the 15q25 locus that were found in European populations were not replicated in Chinese populations, whereas other common variants in 15q25 were identified as susceptibility loci[24]. These findings suggest that there may be a significant difference in lung cancer susceptibility loci between European and Asian populations. Here, we investigated susceptibility loci for lung adenocarcinoma in Japanese and Korean populations.

We conducted a GWAS to identify genes related to lung adenocarcinoma susceptibility in 1,004 Japanese individuals with lung adenocarcinoma and 1,900 without cancer. These samples were genotyped using the Illumina Human610-Quad BeadChip in cases and the Illumina HumanHap550v3 BeadChip in controls. Genotype concordance between these two BeadChips was 99.99% among 182 duplicate samples, indicating a low possibility of genotype error. After we applied stringent quality control criteria, we carried out association analysis in 432,024 autosomal SNPs that were available on both BeadChips. Principal component analysis showed no population substructure in our population (**Supplementary Fig. 1a**). In addition, a quantile-quantile plot using the results of a Cochran-Armitage test showed that the inflation factor, λ, was 1.04, indicating a low possibility of false-positive associations resulting from population stratification (**Supplementary Fig. 1b**).

[1]Laboratory of Molecular Medicine, Human Genome Center, Institute of Medical Science, The University of Tokyo, Tokyo, Japan. [2]Department of Medical Molecular Science, Hiroshima University, Hiroshima, Japan. [3]Laboratory for Genotyping Development, Center for Genomic Medicine, RIKEN, Yokohama, Japan. [4]Laboratory for Statistical Analysis, Center for Genomic Medicine, RIKEN, Yokohama, Japan. [5]Research Institute and Hospital, National Cancer Center, Goyang, Gyeonggi, Korea. [6]Laboratory for Medical Informatics, Center for Genomic Medicine, RIKEN, Yokohama, Japan. [7]Division of Molecular Carcinogenesis, Center for Neurological Diseases and Cancer, Nagoya University Graduate School of Medicine, Nagoya, Japan. [8]Department of Molecular Cytogenetics, Medical Research Institute and School of Biomedical Science, Tokyo Medical and Dental University, Tokyo, Japan. [9]Department of Medical Oncology, Shiga University of Medical Science, Otsu, Japan. [10]Cancer Center, Shiga University of Medical Science Hospital, Otsu, Japan. Correspondence should be addressed to Y.D. (ydaigo@ims.u-tokyo.ac.jp).

Received 12 March; accepted 26 August; published online 26 September 2010; doi:10.1038/ng.667

Table 1 Summary of GWAS and replication studies

SNP	Gene	Study	Allele [1/2]	Case 11	Case 12	Case 22	Control 11	Control 12	Control 22	MAF Case	MAF Control	OR (95%CI)[a]	P^b	P^c_{het}
rs10937405	*TP63*	GWAS	[T/C]	78	400	526	194	854	852	0.277	0.327	1.27 (1.13–1.43)	8.28×10^{-5}	
		1st replication (Japanese)		40	207	276	804	3437	3437	0.274	0.329	1.29 (1.12–1.49)	2.71×10^{-4}	
		2nd replication (Korean)		32	227	301	181	605	666	0.260	0.333	1.42 (1.22–1.66)	1.06×10^{-5}	
		Combined replication studies[d]										1.35 (1.22–1.50)	1.47×10^{-8}	0.37
		Combined all studies[e]										1.31 (1.22–1.42)	7.26×10^{-12}	0.50
rs2736100	*TERT*	GWAS	[A/C]	291	498	215	696	890	314	0.462	0.399	1.29 (1.16–1.44)	5.20×10^{-6}	
		1st replication (Japanese)		157	273	95	2830	3664	1182	0.441	0.393	1.22 (1.08–1.38)	1.92×10^{-3}	
		2nd replication (Korean)		174	277	106	567	692	199	0.439	0.374	1.31 (1.14–1.51)	1.41×10^{-4}	
		Combined replication studies[d]										1.26 (1.15–1.38)	1.48×10^{-6}	0.46
		Combined all studies[e]										1.27 (1.19–1.37)	2.91×10^{-11}	0.71

MAF, minor allele frequency; OR, odds ratio; CI, confidence interval. Odds ratios and *P* values for independence test were calculated by the Mantel-Haenszel method.
[a]Odds ratios of risk allele from two-by-two allele frequency table. [b]*P* value of Cochran-Armitage trend test. [c]Result of Breslow-Day test. [d]Meta-analysis of two replication studies. [e]Meta-analysis of all three studies.

No SNP reached a genome-wide significance level of association ($P < 1 \times 10^{-7}$) in our GWAS (**Supplementary Fig. 1c**). Next, we conducted a replication study using two sample sets: 525 lung adenocarcinoma cases and 7,678 controls for the Japanese set and 569 lung adenocarcinoma cases and 1,470 controls for the Korean set. For the first replication study, we selected 50 SNPs with $P < 1 \times 10^{-4}$ in our GWAS after excluding 12 SNPs with $r^2 \geq 0.8$ in the same locus. As a result, we successfully genotyped all 50 SNPs using the multiplex PCR-based Invader assay and five of them showed $P < 0.05$ with the same risk allele direction (**Supplementary Table 1**). In the second replication study, we genotyped these five SNPs and found two (rs10937405 and rs2736100) that showed $P < 0.05$ (**Table 1**). When we combined the results of the two replication studies using the Mantel-Haenszel method, we found that these two SNPs showed a significant association with lung adenocarcinoma after Bonferroni correction (calculated as $P < 0.05/50$). The first SNP, rs2736100, was located in intron 2 of *TERT*, where we replicated previous findings (combined $P = 2.91 \times 10^{-11}$, OR = 1.27); rs10937405 (combined $P = 7.26 \times 10^{-12}$, OR = 1.31) was located in intron 1 of *TP63* on chromosome 3q28. As shown in **Table 1**, ORs were similar across the three studies and we observed no heterogeneity.

We next analyzed the effect of rs10937405 according to gender and smoking behavior (**Supplementary Table 2**). After combined analysis by the Mantel-Haenszel method, this SNP tended to have higher OR for females than males, but we found no clear trend for smoking behavior. When we analyzed the combined effect of *TP63* and *TERT*, we found that these two susceptibility genes showed a synergistic effect on the risk of lung adenocarcinoma (OR = 4.26; **Supplementary Table 3**).

We also checked the association of other previously reported loci for lung cancer (**Supplementary Table 4**). Although we could not test the association of several SNPs in the loci on chromosomes 6p21.33, 6p22.1, 15q25.1 and 19q13.41 because their minor allele frequencies (MAFs) were too low or zero, our GWAS replicated three loci: rs9840545 in chromosome 3q26.32 ($P = 0.0242$), rs401681 in *CLPTM1L* ($P = 0.0106$) and rs3749971 in *OR12D3* ($P = 0.0241$).

In this study, we identified a new susceptibility locus for lung adenocarcinoma in intron 1 of *TP63* (rs10937405, $P = 7.26 \times 10^{-12}$). *TP63* contains 14 exons and spans about 300 kb. When we constructed linkage disequilibrium (LD) blocks and a $-\log_{10}$ (*P* value) plot around *TP63* using GWAS data, we found that the most associated SNP (rs10937405) represented an LD block that spanned from the upstream exon 1 to intron 1 of *TP63*. This SNP is included in the TP63 isoforms of TAp63 that are transcribed using a promoter upstream of exon 1, but not in other isoforms (ΔNp63) that are regulated by another promoter in intron 3 (ref. 25). To identify causative SNPs, we performed fine mapping of a genomic region containing approximately 200 kb from 190.7 to 190.9 Mb on chromosome 3 using GWAS case-control samples (**Fig. 1**). We used Haploview software to select 64 tag SNPs ($r^2 > 0.9$) on the basis of HapMap Japanese JPT data. We successfully genotyped 63 tagging SNPs in addition to the 45 SNPs already genotyped in GWAS (**Supplementary Table 5**), and we identified three SNPs (rs4488809, rs9816619 and rs4600802) that showed stronger association than rs10937405. Among them, rs4488809 (located 27 kb upstream of the landmark SNP) showed the strongest association. These SNPs were located in neighboring LD blocks and both blocks were located in intron 1 of *TP63* (**Fig. 1**).

Because three other LD blocks upstream of these blocks shared relatively high *D′* values with these blocks, we resequenced a 75-kb region from 190.805 to 190.880 Mb on chromosome 3 using genomic DNA from 96 individuals with lung adenocarcinoma. We identified 11 new SNPs in addition to the 162 known SNPs registered in the dbSNP database and genotyped 4 new SNPs with a MAF ≥ 0.05. However, none of the SNPs showed stronger association than

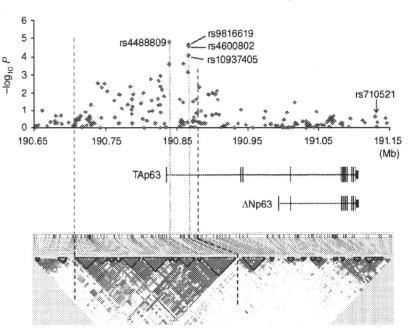

Figure 1 Case-control association plots, LD map and genomic structure of the *TP63* region in chromosome 3q28. The candidate region is shown between two black dotted lines. Fine mapping was performed in the region from 190.7 to 190.9 Mb. Blue diamonds represent $-\log_{10}P$ obtained from the GWAS and fine mapping using GWAS samples. The LD map based on *D′* values was drawn using the genotype data of the cases and controls in GWAS samples. Red dotted line, rs4488809; blue dotted line, landmark SNP (rs10937405); black arrow, rs710521, which shows a significant association with urinary bladder cancer.

rs4488809. We also performed haplotype analysis to investigate the effect of combinations of the four SNPs that were highly associated with lung adenocarcinoma susceptibility; however, no haplotype showed stronger association than the single-marker association of rs4488809 (**Supplementary Fig. 2a**). Although further functional analysis is needed to clarify which SNP is the true causative variant for lung adenocarcinoma, rs4488809 may be a candidate of functional significance.

Recent GWAS for lung cancer and follow-up studies using samples from more than 10,000 samples, mainly of European ancestry, have identified three lung cancer susceptibility loci: 15q24-25.1, which contains genes that encode nicotinic acetylcholine receptor subunits; 5p15.33 (rs2736100, *TERT*; rs401681, *CLPTM1L*); and 6p21.33 (*BAT3–MSH5*)[17–23]. The reasons for the differences between their results and ours might include the existence of unknown causative variant(s) at the same loci that emerged after the European-Asian split and insufficient statistical power due to the difference in MAF between the populations. For example, rs3117582 and rs3131379 in 6p21.33 were not polymorphic in the Japanese population (**Supplementary Table 4**). This may be a case in which the susceptibility variants emerged after the European-Asian split. On the other hand, SNPs in 15q25.1 showed large differences in MAFs between Japanese and European populations. If the true causative variants are linked to rs8034191 or rs1051730, it will be difficult to replicate the association in the Japanese population because of insufficient statistical power due to the low MAF of these SNPs (0.011). Regarding the *TP63* locus, the MAF of the landmark SNP (rs10937405) was similar between European and Japanese populations: MAF = 0.367 in CEU and MAF = 0.322 in JPT in the HapMap database. To investigate whether *TP63* could be a susceptibility locus in European populations, we searched the genotype data of the public lung cancer GWAS dataset from the International Agency for Research on Cancer (IARC)[17]. Genotype data for rs10937405 were not available in the IARC dataset; however, we obtained the genotype data for the alternative SNP, rs4396880, which is highly associated with rs10937405 (r^2 = 0.89 in CEU and 0.95 in JPT in the HapMap database). There was a weak association between rs4396880 and lung cancer in Central European populations with the same risk allele direction (P = 0.0297, OR = 1.11, 95% CI = 1.01–1.21). Although no SNP in this locus was listed in the top 200 SNPs in the meta-analysis of GWAS[23], these data suggest that genetic variation in *TP63* may also influence the susceptibility to lung cancer in European populations.

TP63 (also known as *p63*) is a member of the tumor suppressor *TP53* (also known as *p53*) gene family, which is involved in development, differentiation and response to cellular stress. *TP53* encodes a transcription factor that is essential for the prevention of cancer formation[25]. *TP63* is expressed mainly as two isoforms, the TA and N-terminal-truncated (ΔN) forms. TAp63 isoforms can also transactivate *TP53* target genes[26]. TAp63 isoforms are transcribed using a promoter located upstream of exon 1, whereas expression of the ΔNp63 isoforms are regulated by another promoter in intron 3 (ref. 25). TP63 is induced after exposure of cells to DNA damage[27,28]. Accumulation of DNA damage and lack of response to genotoxic stress contribute to an earlier step in carcinogenesis. Because possible candidate SNPs are located in intron 1 of *TP63*, which encodes TAp63 isoforms, we suggest that one or more of these SNPs may have a functional role in the regulation of *TP63* gene expression. rs710521, located near *TP63*, shows a genome-wide significant association with urinary bladder cancer[29]. Because lung and urinary bladder cancers share common environmental risk factors, such as smoking, we investigated the correlation between SNP rs710521 and those identified in our lung adenocarcinoma study. However, rs710521 was not associated with SNPs identified in our study or with lung adenocarcinoma (P = 0.242; **Fig. 1** and **Supplementary Fig. 2b**).

In summary, our data suggest that *TP63* is a candidate susceptibility gene for lung adenocarcinoma in Japanese and Korean populations. Further functional studies are necessary to clarify the mechanisms by which TP63 influences susceptibility to lung adenocarcinoma. Additional studies on other ethnic populations will also provide detailed information on the genetic etiology and heterogeneity of lung cancer.

METHODS

Methods and any associated references are available in the online version of the paper at http://www.nature.com/naturegenetics/.

Note: Supplementary information is available on the Nature Genetics website.

ACKNOWLEDGMENTS

We thank the staff of the Laboratory for Genotyping Development, Center for Genomic Medicine, RIKEN and the Human Genome Center, Institute of Medical Science, The University of Tokyo for their contribution to SNP genotyping. We also thank members of the BioBank Japan project, the Rotary Club of Osaka-Midosuji District 2660 Rotary International in Japan, and Research Institute and Hospital, National Cancer Center, Korea for supporting our study. Y.D. is a member of the Shiga Cancer Treatment Project supported by Shiga Prefecture (Japan). This work was conducted as a part of the BioBank Japan Project and supported by the Ministry of Education, Culture, Sports, Sciences and Technology of the Japanese government. Management of second replication samples in Korea was supported by grants 0710221 and 0940620 from the National Cancer Center, Korea.

AUTHOR CONTRIBUTIONS

Y.N. conceived the study; D.M., M.K., Y.N. and Y.D. designed the study; D.M., N.H., M.K. and Y.D. performed genotyping; D.M., M.K., Y.N. and Y.D. wrote the manuscript; A.T., T.M., T. Tsunoda and N.K. performed data analysis at the genome-wide phase; Y.N. and M.K. managed DNA samples belong to BioBank Japan: K.-A.Y., J.K., G.-K.L., J.I.Z. and J.S.L. managed second replication samples in Korea: D.M. and Y.D. summarized the results; Y.N., T. Takahashi, K.C., J.I. and Y.D. obtained funding for the study.

COMPETING FINANCIAL INTERESTS

The authors declare no competing financial interests.

Published online at http://www.nature.com/naturegenetics/.
Reprints and permissions information is available online at http://npg.nature.com/reprintsandpermissions/.

1. Jemal, A. *et al.* Cancer statistics, 2009. *CA Cancer J. Clin.* **59**, 225–249 (2009).
2. Parkin, D.M., Bray, F., Ferlay, J. & Pisani, P. Global cancer statistics, 2002. *CA Cancer J. Clin.* **55**, 74–108 (2005).
3. Daigo, Y. & Nakamura, Y. From cancer genomics to thoracic oncology: discovery of new biomarkers and therapeutic targets for lung and esophageal carcinoma. *Gen. Thorac. Cardiovasc. Surg.* **56**, 43–53 (2008).
4. Toyoda, Y., Nakayama, T., Ioka, A. & Tsukuma, H. Trends in lung cancer incidence by histological type in Osaka, Japan. *Jpn. J. Clin. Oncol.* **38**, 534–539 (2008).
5. Sobue, T. *et al.* Trend of lung cancer incidence rate by histological type: a population-based study in Osaka, Japan. *Jpn. J. Cancer Res.* **90**, 6–15 (1999).
6. Thun, M.J. *et al.* Cigarette smoking and changes in the histopathology of lung cancer. *J. Natl. Cancer Inst.* **89**, 1580–1586 (1997).
7. Devesa, S.S., Bray, F., Vizcaino, A.P. & Parkin, D.M. International lung cancer trends by histological type. *Int. J. Cancer* **117**, 294–299 (2005).
8. Janssen-Heijnen, M.L. & Coebergh, J.W. The changing epidemiology of lung cancer in Europe. *Lung Cancer* **41**, 245–258 (2003).
9. Yang, C.H. EGFR tyrosine kinase inhibitors for the treatment of NSCLC in East Asia: present and future. *Lung Cancer* **60** (Suppl. 2), S23–S30 (2008).
10. Jee, S.H., Kim, I.S., Suh, I., Shin, D. & Appel, L.J. Projected mortality from lung cancer in South Korea, 1980–2004. *Int. J. Epidemiol.* **27**, 365–369 (1998).
11. Liam, C.K., Pang, Y.K., Leow, C.H., Poosparajah, S. & Menon, A. Changes in the distribution of lung cancer cell types and patient demography in a developing multiracial Asian country: experience of a university teaching hospital. *Lung Cancer* **53**, 23–30 (2006).
12. Fukuoka, M. *et al.* Multi-institutional randomized phase II trial of gefitinib for previously treated patients with advanced non-small-cell lung cancer. *J. Clin. Oncol.* **21**, 2237–2246 (2003).

13. Huang, S.F. *et al.* High frequency of epidermal growth factor receptor mutations with complex patterns in non-small cell lung cancers related to gefitinib responsiveness in Taiwan. *Clin. Cancer Res.* **10**, 8195–8203 (2004).
14. Marchetti, A. *et al.* EGFR mutations in non-small-cell lung cancer. *J. Clin. Oncol.* **23**, 857–865 (2005).
15. Matakidou, A., Eisen, T. & Houlston, R.S. Systematic review of the relationship between family history and lung cancer risk. *Br. J. Cancer* **93**, 825–833 (2005).
16. Zhang, Y. *et al.* Family history of cancer and risk of lung cancer among nonsmoking Chinese women. *Cancer Epidemiol. Biomarkers Prev.* **16**, 2432–2435 (2007).
17. Hung, R.J. *et al.* A susceptibility locus for lung cancer maps to nicotinic acetylcholine receptor subunit genes on 15q25. *Nature* **452**, 633–637 (2008).
18. Amos, C.I. *et al.* Genome-wide association scan of tag SNPs identifies a susceptibility locus for lung cancer at 15q25.1. *Nat. Genet.* **40**, 616–622 (2008).
19. Thorgeirsson, T.E. *et al.* A variant associated with nicotine dependence, lung cancer and peripheral arterial disease. *Nature* **452**, 638–642 (2008).
20. McKay, J.D. *et al.* Lung cancer susceptibility locus at 5p15.33. *Nat. Genet.* **40**, 1404–1406 (2008).
21. Wang, Y. *et al.* Common 5p15.33 and 6p21.33 variants influence lung cancer risk. *Nat. Genet.* **40**, 1407–1409 (2008).
22. Broderick, P. *et al.* Deciphering the impact of common genetic variation on lung cancer risk: a genome-wide association study. *Cancer Res.* **69**, 6633–6641 (2009).
23. Landi, M.T. *et al.* A genome-wide association study of lung cancer identifies a region of chromosome 5p15 associated with risk for adenocarcinoma. *Am. J. Hum. Genet.* **85**, 679–691 (2009).
24. Wu, C. *et al.* Genetic variants on chromosome 15q25 associated with lung cancer risk in Chinese populations. *Cancer Res.* **69**, 5065–5072 (2009).
25. Moll, U.M. & Slade, N. p63 and p73: roles in development and tumor formation. *Mol. Cancer Res.* **2**, 371–386 (2004).
26. Flores, E.R. The roles of p63 in cancer. *Cell Cycle* **6**, 300–304 (2007).
27. Katoh, I., Aisaki, K., Kurata, S., Ikawa, S. & Ikawa, Y. p51A (TAp63gamma), a p53 homolog, accumulates in response to DNA damage for cell regulation. *Oncogene* **19**, 3126–3130 (2000).
28. Petitjean, A. *et al.* Properties of the six isoforms of p63: p53-like regulation in response to genotoxic stress and cross talk with DeltaNp73. *Carcinogenesis* **29**, 273–281 (2008).
29. Kiemeney, L.A. *et al.* Sequence variant on 8q24 confers susceptibility to urinary bladder cancer. *Nat. Genet.* **40**, 1307–1312 (2008).

ONLINE METHODS

Samples. Characteristics of each case-control group are shown in **Supplementary Table 6**. Case and control samples used in this study for the Japanese population were obtained from BioBank Japan at the Institute of Medical Science, The University of Tokyo[30]. From the registered samples in BioBank Japan, we selected 1,551 individuals who were pathologically diagnosed as having lung adenocarcinoma. We used 1,026 samples as a set for the GWAS and an independent 525 samples as a set for the first replication study. The control groups included 994 samples for the GWAS and an independent 7,678 samples as a set for the first replication study. All the control samples were GWAS samples for other diseases in the BioBank Japan project. We excluded control samples that were registered for any cancer. We also obtained 906 Japanese control DNAs that were analyzed in the GWAS from volunteers without cancer from the Osaka-Midosuji Rotary Club, Osaka, Japan. Lung adenocarcinoma cases and controls obtained for the second replication study in the Korean population (n = 569 and 1,470, respectively) were obtained from the National Cancer Center, Korea. All participants provided written informed consent. This project was approved by the ethical committees of each participating institution.

SNP genotyping. Genomic DNA was extracted from peripheral blood leukocytes using a standard method. For the GWAS, we genotyped 1,026 cases using Illumina HumanHap610-Quad BeadChip and 1,900 controls using the Illumina HumanHap550v3 Genotyping BeadChip. After we excluded 22 samples with call rate <0.98, we applied SNP quality control (call rate ≥0.99 in both cases and controls, a MAF ≥0.01 and a P value in the Hardy-Weinberg equilibrium test of $\geq 1.0 \times 10^{-6}$ in controls): 432,024 SNPs in autosomal chromosomes passed the quality control filters and were further analyzed. We used genome-wide screening data for other diseases (chronic hepatitis B, keloid, drug rash, febrile seizure and pulmonary tuberculosis) as controls for the GWAS, which were genotyped using the Illumina HumanHap550v3 Genotyping BeadChip. For controls for the first replication study in the Japanese population, we also used genome-wide screening data for diabetes, peripheral artery disease, arrhythmias, stroke and myocardial infarction, which were genotyped using the Illumina HumanHap610 Genotyping BeadChip and applied the same quality control criteria as for the GWAS.

We used multiplex-PCR based Invader assays (Third Wave Technologies) for the replication studies of Japanese and Korean populations and also for fine mapping[31].

Fine mapping and resequencing. We performed fine mapping using all case and control samples in GWAS. Haploview was used to select tag SNPs with a pairwise $r^2 > 0.90$ and a MAF ≥0.05 on the basis of HapMap JPT data. Resequencing of candidate regions was performed in 96 lung adenocarcinoma cases using an ABI3730 Genetic Analyzer.

Statistical analysis. In GWAS and the first and second replication studies in Japanese and Korean populations, the statistical significance of the association with each SNP was assessed using a 1-degree-of-freedom Cochran-Armitage trend test. OR and CI were calculated from a two-by-two allele frequency table. Combined analysis was performed using the Mantel-Haenszel method. Heterogeneity among studies was examined using the Breslow-Day test. We used Haploview software to analyze the association of haplotypes and LD values between *TP63* and SNPs.

Software. For general statistical analyses, we used the R statistical environment version 2.6.1 or PLINK1.03 (ref. 32). To draw the LD map and analyze the association of haplotypes, we used Haploview software[33].

URLs. PLINK1.03, http://pngu.mgh.harvard.edu/~purcell/plink/; R statistical environment, http://www.cran.r-project.org/; IARC lung cancer database, http://www.cng.fr/prog_cancergenomics/lung_cancer.html.

30. Nakamura, Y. The BioBank Japan project. *Clin. Adv. Hematol. Oncol.* **5**, 696–697 (2007).
31. Ohnishi, Y. *et al.* A high-throughput SNP typing system for genome-wide association studies. *J. Hum. Genet.* **46**, 471–477 (2001).
32. Purcell, S. *et al.* PLINK: a tool set for whole-genome association and population-based linkage analyses. *Am. J. Hum. Genet.* **81**, 559–575 (2007).
33. Barrett, J.C., Fry, B., Maller, J. & Daly, M. Haploview: analysis and visualization of LD and haplotype maps. *Bioinformatics* **21**, 263–265 (2005).

Laboratory Investigation (2010) 90, 360–373

Homozygous deletion of *CDKN2A/2B* is a hallmark of iron-induced high-grade rat mesothelioma

Qian Hu[1,2], Shinya Akatsuka[1], Yoriko Yamashita[1], Hiroki Ohara[1,2], Hirotaka Nagai[1,2], Yasumasa Okazaki[1], Takashi Takahashi[3] and Shinya Toyokuni[1,*]

In humans, mesothelioma has been linked to asbestos exposure, especially crocidolite and amosite asbestos, which contain high amounts of iron. Previously, we established a rat model of iron-induced peritoneal mesothelioma with repeated intraperitoneal injections of iron saccharate and an iron chelator, nitrilotriacetate. Here, we analyze these mesotheliomas using array-based comparative genomic hybridization (aCGH) and gene expression profiling by microarray. Mesotheliomas were classified into two distinct types after pathologic evaluation by immunohistochemistry. The major type, epithelioid mesothelioma (EM), originated in the vicinity of tunica vaginalis testis, expanded into the upper peritoneal cavity and exhibited papillary growth and intense podoplanin immunopositivity. The minor type, sarcomatoid mesothelioma (SM), originated from intraperitoneal organs and exhibited prominent invasiveness and lethality. Both mesothelioma types showed male preponderance. SMs revealed massive genomic alterations after aCGH analysis, including homozygous deletion of *CDKN2A/2B* and amplification of *ERBB2* containing region, whereas EMs showed less genomic alterations. Uromodulin was highly expressed in most of the cases. After 4-week treatment, iron deposition in the mesothelia was observed with 8-hydroxy-2′-deoxyguanosine formation. These results not only show two distinct molecular pathways for iron-induced peritoneal mesothelioma, but also support the hypothesis that oxidative stress by iron overload is a major cause of *CDKN2A/2B* homozygous deletion.
Laboratory Investigation (2010) **90,** 360–373; doi:10.1038/labinvest.2009.140; published online 11 January 2010

KEYWORDS: iron; mesothelioma; oxidative stress; *CDKN2A/2B*; *ERBB2*; uromodulin

Iron is universally abundant. During evolutionary processes, vertebrates have selected iron as a carrier of oxygen (hemoglobin) inside the body. However, iron represents a double-edged sword as excess levels increase the risk for cancer, presumably through the generation of reactive oxygen species (ROS).[1] Thus far, pathological conditions such as those resulting from asbestos fiber exposure as well as hemochromatosis, chronic viral hepatitis B and C, and endometriosis have been recognized as iron overload-associated risks for human cancers.[2]

Respiratory exposure to asbestos fibers has been associated with diffuse malignant mesothelioma in humans. Despite advancements in the molecular analysis of human mesothelioma and in the development of animal models, the carcinogenic mechanisms of the disease remain unclear. Mesothelioma with poor prognosis continues to be a serious social problem in many countries.[3] Therefore, it is important to elucidate the carcinogenic mechanisms of mesothelioma in order to establish techniques for early diagnosis and to develop preventive strategies for people exposed to asbestos. Currently, three hypotheses exist regarding the pathogenesis of asbestos-induced mesothelioma.[4] The 'oxidative stress theory'[5] is based on the fact that fibrous mineral foreign substances in asbestos are phagocytosed by macrophages, which are unable to digest them, resulting in the massive generation of ROS. Alternatively, crocidolite and amosite may present catalyzing reactive environments with exposed surface iron. Consistent with this hypothesis, epidemiological studies indicate that asbestos fibers containing iron are more carcinogenic.[6] The 'chromosome tangling theory' postulates that asbestos fibers damage chromosomes when cells divide.[7] Finally, the 'molecular adsorption theory' states that a variety

[1]Department of Pathology and Biological Responses, Nagoya University Graduate School of Medicine, Nagoya, Japan; [2]Department of Pathology and Biology of Diseases, Graduate School of Medicine, Kyoto University, Kyoto, Japan and [3]Department of Tumor Biology, Nagoya University Graduate School of Medicine, Nagoya, Japan
*Correspondence: Professor S Toyokuni, MD, PhD, Department of Pathology and Biological Responses, Nagoya University Graduate School of Medicine, 65 Tsurumai-cho, Showa-ku, Nagoya, Aichi 466-8550, Japan.
E-mail: toyokuni@med.nagoya-u.ac.jp

Received 4 July 2009; revised 24 October 2009; accepted 16 November 2009

of proteins and chemicals including components of cigarette smoke bind to the broad surface area of asbestos.[5] This might result in the accumulation of hazardous molecules.

The first hypothesis stresses the importance of local iron overload in the carcinogenic process of mesothelioma. In 1989, we succeeded in producing a rat model of peritoneal mesothelioma using ferric saccharate followed by administration of an iron chelator, nitrilotriacetate. This model demonstrated, for the first time, that local iron deposition is an important factor in the generation of diffuse malignant mesothelioma.[8] In this study, we have applied two microarray techniques to these iron-induced peritoneal mesotheliomas to elucidate the molecular mechanisms of iron-induced mesothelial carcinogenesis.

MATERIALS AND METHODS

Animal Experiments and Chemicals

The carcinogenesis study was performed as previously described[8] with slight modification, using specific pathogen-free F1 hybrid rats crossed between Fischer344 (F344; female) and Brown-Norway (BN/CIJ; male) strains (Charles River, Yokohama, Japan). In some acute and subacute experiments, specific pathogen-free male Wistar rats (Shizuoka Laboratory Animal Center, Shizuoka, Japan) were also used. Animals were fed a basal diet (Funabashi F-1; Funabashi, Chiba, Japan) and tap water *ad libitum*. Ferric saccharate (Fesin; Yoshitomi Pharmaceutical Company, Osaka, Japan) was prepared in a 5% glucose solution. The nitrilotriacetic acid (NTA) solution was prepared by dissolving NTA, disodium salt (Nakalai Tesque, Kyoto, Japan), in physiological saline, and the pH was adjusted using sodium bicarbonate to pH 7.4. For the carcinogenesis study, a total of 92 F1 hybrid rats were divided into two groups of untreated control ($N=38$) and iron-treated ($N=54$). The injections were started at 4 weeks of age. Ferric saccharate (5 mg iron/kg body weight) was injected intraperitoneally 5 days a week for 12 weeks. NTA (80 mg/kg body weight) was administered separately intraperitoneally 5 days a week for 20 weeks. This form of iron primarily deposits in the peritoneum.[8] The animals were kept under close observation and were killed when they showed persistent weight loss and/or distress. The experiments were terminated at 26.7 months of age. All the animals were autopsied. Samples were either immediately frozen and stored at $-80^{\circ}C$ until use, or subjected to routine histological analysis with buffered 10% formalin fixation and paraffin embedding. The animal experiment committees of the Graduate School of Medicine, Kyoto University and Nagoya University Graduate School of Medicine approved these animal experiments. All chemicals used were of analytical quality.

Rat Peritoneal Mesothelial Cells

Rat peritoneal mesothelial cells (RPMC) were cultured from the omentum of Wistar rats as previously described,[9] and grown in RPMI 1640 medium containing 10% fetal calf serum. A retroviral vector pCMSCVpuro-16E6E7 was constructed by recombining the segment of a donor vector containing full-length HPV16E6 and E7 (A kind gift from Dr Tohru Kiyono, National Cancer Center, Tokyo, Japan) into the destination vector by the Gateway System (Invitrogen Life Technologies, Carlsbad, CA, USA) as described previously.[10] RPMCs were infected at day 14 by the recombinant retrovirus expressing the 10A1 envelope[11] with 4 μg/ml polybrene, and were drug selected using 1 μg/ml puromycin.

Array-Based CGH Analysis

We performed array-based comparative genomic hybridization (aCGH) with a Rat Genome CGH Microarray 244A (G4435A; Agilent Technologies, Santa Clara, CA, USA), as described in the Agilent Oligonucleotide Array-based CGH for Genomic DNA Analysis Protocol ver. 5.0, and analyzed results with DNA Analytics Software (ver. 4.0). For each array, normal kidney was used as a reference and labeled with Cy-3. Samples of interest were labeled with Cy-5. Six cases of epithelioid mesotheliomas (EMs) and five cases of sarcomatoid mesotheliomas (SMs) were analyzed.

Fluorescent *In Situ* Hybridization

Appropriate bacterial artificial chromosome probes were selected from http://genome.ucsc.edu/ and purchased from http://bacpac.chori.org/. CH230-163D24 was used for *CDKN2A/2B*, and CH230-209G15 for *Erbb2*. Fluorescent probes were labeled by incorporating Green-dUTP (Vysis; Abbott Laboratories; Abott Park, IL, USA) into newly synthesized DNA by the Nick Translation Kit (Vysis). Fluorescent *in situ* hybridization (FISH) was performed using the probes, Paraffin Pretreatment Kit and LSI/WCP Hybridization Buffer (Vysis) according to the manufacturer's protocol. Briefly, paraffin sections were treated with protease, and after denaturation, the probes were hybridized to nuclear DNA, counterstained with DAPI, and visualized using a fluorescence microscope.

Expression Microarray Analysis

A total of 12 microarrays (Whole Rat Genome Microarray, G4131F; Agilent Technologies) were used for the screening purpose: four chips were used for tooth brush-scraped pleural and peritoneal mesothelial cells and soft tissue surrounding tunica vaginalis testis, six for EMs and two for SMs. Total RNA was isolated with an RNeasy Mini kit (QIAGEN GmbH, Hilden, Germany). Data analysis was performed using GeneSpring GX 10.02.2 software (Agilent Technologies).

Quantitative RT-PCR Analysis

Total RNA was extracted with RNeasy Mini (QIAGEN) and cDNA was synthesized using SuperScript III First-strand Synthesis System for RT-PCR (Invitrogen Life Technologies) with random primers. All of the primers used are summarized in the Supplementary Table 1.

Antibody

An anti-uromodulin rabbit polyclonal antibody was produced by a commercial supplier (Hokudo, Hokkaido, Japan). Briefly, a 15-mer polypeptide (NH_3-CKQDFNVTDVSLLEH-COOH) corresponding to the 320-334 cytoplasmic portion of rat UMOD protein (AAH81814) was synthesized and conjugated with keyhole limpet hemocyanin, which was used as an immunogen for JW rabbits. Five weeks after the second immunization, whole serum was harvested and purified using a SulfoLink Kit (Pierce, Rockford, IL, USA). Anti-S-100 polyclonal antibody (LSL-LB-9197) was from Cosmo Bio (Tokyo, Japan). Anti-desmin monoclonal antibody (clone D33) was from DAKO (Carpinteria, CA, USA). Anti-podoplanin polyclonal antibody (KS-17) was from Sigma (Saint Louis, MO, USA). Anti-multi-cytokeratin monoclonal antibody (RTU-AE1/AE3) was from Novocastra (Newcastle, UK). Anti-8-hydroxy-2′-deoxygunosine monoclonal antibody (clone N45.1)[12] was from Nikken Seil (Shizuoka, Japan). Anti-single stranded DNA antibody (no. 18731) was from IBL (Takasaki, Gunma, Japan).

Western Blot Analysis

This was performed using a standard procedure as previously described.[13,14]

Histology, Tissue Array, and Immunohistochemical Analysis

The specimens embedded in paraffin were cut at 3-μm thickness, stained with hematoxylin and eosin, or used for immunohistochemistry. Representative areas were chosen and cores of 3 mm diameter were punched out from the blocks with a precision instrument (Tissue Microprocessor; Azumaya, Tokyo, Japan). Those cores of 24 (6 × 4 array) in a group were embedded in a paraffin block. Immunohistochemistry was performed as previously described.[12] Antigen retrieval for single-stranded DNA was by incubation with proteinase K solution (Trevigen, Gaithersburg, MD, USA) at 37°C for 30 min. Negative controls are shown in the Supplementary Figure 1.

Detection of DNA-Strand Breaks

TUNEL (terminal deoxynucleotidyl transferase-mediated dUTP nick end labeling; TACS 2 TdT-Blue Label *In situ* Apoptosis Detection kit; Trevigen) method and immunohistochemical analysis for single-stranded DNA were used.

Statistical Analysis

Statistical analyses were performed with an unpaired *t*-test, which was modified for unequal variances when necessary. Kaplan–Meier analysis was also used. $P < 0.05$ was considered as statistically significant.

RESULTS

Two Distinct Pathologies were Observed in Ferric Saccharate-Induced Rat Peritoneal Mesothelioma

F1 hybrids between Fischer344 and Brown-Norway rat strains were used to allow allele-specific analyses when necessary. There was no significant difference in the survival between the control and iron-injected groups up to 20 months of age. Thereafter, animals in the iron-treatment group started to die from mesothelioma (Figure 1). Control animals generated no mesothelioma during the 26.7-month postnatal observation period. All observed tumors are summarized in Tables 1 and 2.

Two distinct pathologies were observed in the obtained mesotheliomas. The majority of tumors were observed in the vicinity of tunica vaginalis testis, and expanded to the upper peritoneal cavity in half of the cases (Figure 2). Most of the animals did not die from the disease during the observation period. When fine tumors were scattered throughout the whole peritoneum, we recognized these as malignant. Such tumors revealed papillary growth patterns and were always intensely positive for podoplanin and cytokeratin (Figure 2). These tumors were counterparts of human EM.

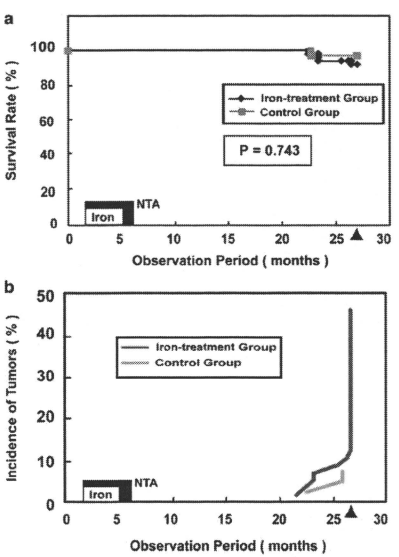

Figure 1 Survival rates (**a**) and incidence of tumors (**b**) in the iron-treatment group (iron saccharate followed by nitrilotriacetic acid) and the untreated control group. The arrow head shows the point of experiment termination (26.7 months after birth). NTA, nitrilotriacetic acid. Refer to Materials and methods section for details.